Brazilian Journal of Geophysics 42 (2024), 1, 1-30
Brazilian Geophysical Society
ISSN 2764-8044
DOI: 10.22564/brjg.v41i2.2300

COMBINATION OF FOURIER AND CRS-BASED RECONSTRUCTION ALGORITHMS IN LAND SEISMIC DATA

Yuri S.F. Bezerra[1], German Garabito[1], and Mauricio Sacchi[2]

[1]Universidade Federal do Rio Grande do Norte – UFRN, Natal, RN, Brazil

[2]University of Alberta, Department of Physics, Edmonton, Alberta, Canada

*Corresponding author email: yuri.bezerra.052@ufrn.edu.br

ABSTRACT.
The reconstruction based on the partial CRS stacking operator presents higher signal-to-noise ratio and better continuity of events. However, irregularly sampled land data often introduce errors in the CRS attributes, creating artifacts that contaminate the seismic data. Recently, the combination of Fourier and CRS-based reconstruction algorithms has significantly solved these problems. The approach consists of applying a Fourier-based interpolation method as a regularization operator to the original data and then the CRS attributes are searched in the reconstructed data. The CRS attributes determined in this way are more accurate and they can be applied in two different forms, either in the interpolation and regularization of the original data or in the denoising of the Fourier-based reconstructed data. We propose to compare the combination of the Fourier-based interpolation methods MWNI and MPFI with the CRS-based interpolation method in order to evaluate which is the best preconditioner of the prestack data to search the CRS attributes. We applied the proposed flowcharts combining the interpolation methods mentioned above to the land seismic data from the Tacutu basin, which is vintage data with very low fold and noisy. The reconstructed data obtained by the combinations show significant improvements compared to the data reconstructed using the algorithms separately, in other words, the weaknesses and limitations of each method are overcome when they are applied in combination. The MWNI+CRS combination flow produces the best results, with the stacked section of reconstructed data showing better noise removal, enhancement of coherent events, better definition and continuity of steeply dipping events.

Keywords: Land Seismic Data, Processing, Regularization, Interpolation, Imaging

INTRODUCTION

Reconstruction of seismic data is used in estimating missing traces, filling gaps between shots and increasing the signal-to-noise ratio of surveys (Schonewille *et al.*, 2003, 2009). Reconstruction methods also serve to homogenize fold and to assemble datasets with a regular distribution of azimuths and with an attenuated acquisition footprint (Hunt *et al.*, 2010). Several multidimensional methods for regularization and interpolation of seismic data are currently available. Most popular methods are those based on Fourier kernels, such as Minimum Weighted Norm Interpolation (MWNI) (Liu and Sacchi, 2004), Anti-Leakage Fourier Transform (ALFT) (Xu *et al.*, 2005), Matching Pursuit Fourier Interpolation (MPFI) (Nguyen and Winnett, 2011), and Projection Onto Convex Sets (POCS) interpolation (Abma and Kabir, 2006).

The Common Reflection Surface (CRS) stack operator and its wavefront attributes were adopted for prestack data interpolation and regularization (Hoecht *et al.*, 2009; Baykulov and Gajewski, 2009). CRS-based interpolation generally produces prestack data with high signal-to-noise ratio and enhanced reflections. Contrary to Fourier-based methods, which are inherently signal processing tools, CRS methods are based on kinematic propagation models, and therefore, they incorporate approximated wave propagation physics into reconstruction. Hoecht *et al.* (2009) introduced two interpolation schemes, target-oriented and operator-oriented methods, using the finite-offset CRS stack operator. These methods were successfully applied to synthetic and field data examples. Similarly, Baykulov and Gajewski (2009) proposed a 2D prestack data interpolation and enhancement algorithm called partial CRS stack, which uses the zero-offset CRS stacking operator.

Several studies have demonstrated the potential of CRS-based reconstruction to improve the results of other known applications. Soleimani and Roshandel Kahoo (2016) combined CRS-based interpolation and a trace distribution method to fill gaps and estimate a regular distribution of traces across all bins and azimuths of 3D seismic data. In other words, the seismic traces are interpolated in areas with gaps by CRS-based interpolation. Then these traces are distributed throughout the empty bins applying a trace distribution method that allocates interpolated traces to selected bins. Garabito *et al.* (2021) combined CRS-based prestack data regularization and reverse time migration (RTM). They show that the combi-

nation of CRS interpolation and RTM is adequate to produce high-quality results from low-quality land data. Muhtar *et al.* (2021) applied regularization and interpolation by including the wavefront attributes based on the CRS method before the velocity variation with azimuth (VVAz) inversion. Based on the evaluation of the 3D seismic data after regularization, the amplitude versus offset (AVO) phenomena, and the VVAz inversion results are relatively consistent with the model. A similar result is found for the case of real 3D seismic data.

To apply the interpolation algorithm called partial CRS stacking, the wavefront attributes must initially be extracted from the data. Low-quality land seismic data, with missing traces and large gaps between shots, can negatively impact the search for wavefront attributes. The latter can lead to the generation of false events that contaminate seismic images. These false events appear as artifacts in the stacked and migrated images, destroying the continuity of reflectors. Due to these problems, some authors have proposed new strategies to improve the estimation of wavefront kinematic attributes. Schwarz *et al.* (2015), have proposed an extension of the standard scheme for obtaining CRS attributes. They also include slope information that is extracted from surfaces with zero-offset. They showed, with simple synthetic examples and for complex field data from the eastern Mediterranean, that the presented method allows efficient analysis and refinement of the entire prestack slope, which can help to further automate the picking-intensive process of stereotomography.

Recently, Rad and Hickey (2022) studied the processing of shallow seismic data applying a strategy that combines mute and CRS reconstruction. They showed that the CRS method can improve processing of near-surface seismic data by improving prestack gathers, semblance picking for velocity model building, and zero-offset stacked data. CRS-based local stacking was able to mitigate the data loss associated with optimum-windowing based muting of coherent noise. In addition, the enhanced CRS-based data enables improved near-surface velocity model building, producing higher coherence and more focused semblance peaks. The CRS stacking shown to higher smoothness and provide more continuity of events in the zero-offset data. Applications to a synthetic and two-field dataset collected in high and low velocity environments show the efficiency and feasibility of the proposed approach.

To overcome the limitations of CRS-based interpolation, such as the generation of false coherent events or artifacts due to large gaps in the data, Bezerra *et al.* (2021) proposed a new workflow, combining the MPFI interpolation algorithm based on Fourier reconstruction and CRS-based prestack data interpolation. The results showed a significant improvement of the Tacutu basin data in relation to the combined algorithms applied separately, better solving steep curvature events. This methodology has formalized and expanded by Bezerra *et al.* (2022), along with the presentation of another similar workflow, where CRS-based interpolation is applied to the original data, with the preconditioned CRS attributes obtained from the reconstructed data by the MWNI algorithm. The results shown a significant improvement of the Parnaíba basin data where the gaps are filled in more correctly. Moreover, shallow reflections show better continuity.

We propose a comparative study with these new processing workflows to identify the advantages and drawbacks of the MWNI and MPFI algorithms to precondition the input data before searching for the CRS wavefront attributes. We also compare the CRS-based regularization and interpolation using the wavefront attributes extracted from the original and preconditioned data. Furthermore, we employ CRS-based reconstruction to data preconditioned via MWNI and MPFI methods. We adopted the PSTM migration image as the main metric to evaluate the reconstruction quality and the RMSE and SNR metrics to quantitatively evaluate the results of all algorithms. We present a brief review of the all data reconstruction methods and apply it to the seismic line acquired in the Tacutu onshore Brazilian basin. The interpolation and regularization of this particular dataset is a challenge because of its low signal-to-noise ratio and complex geology.

METHODOLOGY

This section briefly describes all methods used in this study. First, we will introduce the reconstruction domains used by each method. Next, we present the three reconstruction methods in the following order MWNI, MPFI and CRS-based interpolation. Finally, we present the two workflows used for comparisons.

Reconstruction Domains

The Fourier transform-based reconstruction methods, specifically the MWNI and MPFI, operate in the frequency-wavenumber (f-k) domain. Data is mapped from the time-space (t-x) to the frequency-space (f-x) domain by the 1D Fourier transform. The source-receiver reconstruction coordinates were adopted for both Fourier-based algorithms. In the MWNI and MPFI algorithms, the interpolation effectively occurs in the spatial coordinate for one frequency slice at a time, i.e. in the f-k domain. After completing the reconstruction, the data is mapped back to the t-x domain, using the inverse Fourier transform.

In sampling subsurface seismic events, only a certain range of the entire available frequency band is relevant for the reconstruction of seismic data. To optimize the processing of seismic data reconstruction in the f-x domain, frequency limits must be chosen carefully. If the frequency range used is too wide, this can result in higher (unnecessary) computational costs, because using very high frequencies, which normally have low amplitudes, will not improve the reconstructions events. Conversely, if a very short frequency range is used, smaller than the frequency content or frequency band of the data, significant signal losses will occur.

With regard to the reconstruction of prestack data based on the CRS stacking method, all the processes involved are carried out in the t-x domain. In other word, the search for the wavefront attributes of the CRS operator and the partial CRS stacking interpolation are performed in the same t-x domain.

Minimum Weighted Norm Interpolation (MWNI)

The MWNI algorithm is applied in the frequency-wavenumber (f-k) domain. The Fourier coefficients that model the data are estimated by regularized inversion, for each frequency slice. In general, MWNI and all Fourier-based reconstruction algorithms are applied on space-time windows to minimize the number of dips (wavenumbers) that the algorithm needs to iteratively retrieved (Sacchi *et al.*, 1998; Zwartjes and Gisolf, 2007; Stanton and Sacchi, 2013).

The MWNI requires regularly gridded input data. The latter permits the use of the Fast Fourier Transform (FFT) in its inversion kernel. The MWNI algorithm entails solving an inverse problem that include a wavenumber domain regularization term. It minimizes a wavenumber weighted norm that incorporates *a prior* spectral signature of the unknown k-space data spectrum (Liu and Sacchi, 2004). The problem is solved via the Iteratively Reweighted Least-Squares (IRLS) method with inner solver given by the Conjugate Gradient (CG) method. The method is fully iterative and replaces Matrix-time-vector multiplications by fast operations using FFTs (Zwartjes and Sacchi, 2007; Trad, 2014). The MWNI algorithm can be summarized as follows:

1. Initialize the weighting matrix as the identity matrix. This constrains all wavenumbers within the Fourier support.
2. Starting IRLS loop with the initial model equal to zero, where the model is the Fourier optimal spectrum.
3. Find the new approximation to the Fourier spectrum using the CG scheme.
4. Update the weighting matrix using the model found by CG scheme.
5. Use the model found by CG scheme in the new IRLS iteration as the initial model.
6. Repeat steps 2 to 5 until it reaches the maximum number of iterations defined or a desired misfit.

The IRLS algorithm, involves solving the problem for a known weighting matrix via the conjugate gradient method. After the weight matrix is updated, the problem is solved again via the conjugate gradient

method (Zwartjes and Sacchi, 2007). To return from the f-x domain, an inverse FFT is used to estimate data in t-x. In general, the CG method (interior loop of IRLS) converges to a solution in a few iterations (Chiu, 2014).

Matching Pursuit Fourier Interpolation (MPFI)

The Matching Pursuit method is a sparse approximation algorithm that seeks to find the best match projections between data and a redundant expansion of a given dictionary, where the dictionary can be a collection of parameterized waveforms. In seismic interpolation, the main applications use a dictionary formed by expanding the Fourier transform kernel (Mallat and Zhang, 1993). According to Schonewille *et al.* (2013), the MPFI algorithm is an alternative to algorithms that use binning, such as MWNI, as they present better results in noisy data and with complex coordinates. The Matching Pursuit algorithm has been used widely in signal processing, and its main properties are well understood, such as the convergence of the algorithm for any function in the space covered by the dictionary, the monotonic decrease in error at each step, and the energy conservation equation is satisfied at each step (Nguyen and Winnett, 2011).

The input prestack data to the MPFI algorithm is organized in the true acquisition coordinates; that is, it does not need to be previously binned for a regular grid. The flexibility of MPFI to reconstruct the input data for any desired grid is a major attraction. Because MPFI uses Nonuniform Discrete Fourier Transform (NDFT) in each iteration, it becomes computationally expensive in multidimensional interpolation, a significant disadvantage about algorithms that use FFT, as the MWNI and POCS. Assuming that few Fourier components represent regularly sampled data, that is, sparse representation of data in the Fourier domain, the MPFI uses a greedy algorithm to solve one wavenumber per iteration, increasing flexibility for noise attenuation. For each frequency slice of the f-x domain, they transform to f-k domain, find the maximum energy Fourier coefficients, apply the matching pursuit estimated model, iteratively, and back to f-x domain.

The procedure to be performed by the MPFI algorithm can be described as follows:

1. Initialize all components of the Fourier optimal spectrum equal to zero.

2. Compute the Fourier spectrum of the input data using the forward NDFT.

3. Find the wavenumber corresponding to the highest energy coefficient and compute the Fourier coefficient corresponding to this wavenumber.

4. Update the input data by subtracting the contribution of the estimated optimally coefficient.

5. Repeat steps 2 to 4 until the residual input data to be less than a defined maximum error or until the algorithm reaches the maximum number of iterations.

An inverse NDFT of the Fourier optimal spectrum is applied to back to the f-x domain. After going through all the frequencies, the reconstructed data can be back to the t-x domain using the inverse 1D FFT. The stopping criteria are when the residual norm is less than 10^{-2} or the maximum number of iterations is met.

CRS-Based Interpolation

One of the most useful applications of the Common Reflection Surface (CRS) stacking operator is interpolation and enhancement of prestack data (Hoecht *et al.*, 2009; Garabito, 2018; Garabito *et al.*, 2021). The CRS stacking method was introduced to simulate Zero-Offset (ZO) stacked data from multi-coverage seismic data, i.e. approximates the true reflection traveltimes in the midpoint-offset coordinates. Its main products are three sections of wavefront kinematic attributes (known as CRS attributes) that can be applied to a variety of seismic reflection problems. The CRS attributes are the ZO central ray's emergence angle, the normal incidence point (NIP) wave and normal wave curvatures. These three wavefront attributes are determined by employing global optimization, using as an objective function the measure of coherence (semblance) of the seismic signal in the prestack data. Once these CRS attributes are known for a given time sample point in the ZO plane, the CRS stacking surface is constructed. To simulate a ZO stacked section with the CRS stack method, the amplitudes of the seismic traces are summed, and the

result is placed at the evaluated point.

The interpolation algorithm introduced by Baykulov and Gajewski (2009) used the CRS operator locally and centred on the target trace located in the midpoint-offset coordinates to sum the amplitudes of neighbouring traces and build the interpolated trace. The three attributes that define the CRS operator are extracted from the prestack data by applying an automatic search based on the coherence measure of the seismic signal. In the applications presented in this work, we will use the global strategy proposed in Garabito *et al.* (2012) to search the three CRS attributes simultaneously. A global optimization strategy ensures good accuracy of the three CRS attributes, leading to more confident and high-quality results when applied in seismic problems, such as prestack data interpolation, determination of the velocity model, prestack migration, etc. However, the CRS attributes can lead to false coherent events in places where the data has spatial sampling problems.

The CRS-based interpolation algorithm can be summarized as:

1. Determination of the three CRS attributes from prestack data.
2. For a target trace in the midpoint-offset coordinates and a given time sample, define the partial CRS stack operator.
3. Sum of the amplitudes over the partial CRS stack operator and place the result to the point located in the center of the stacking operator.
4. Repeat the operation from step 3 for the entire target trace.
5. Repeating steps 2 to 4 for all traces with constant offset of the seismic line, a common-offset (CO) gather is interpolated and enhanced.

Applying the algorithm described above, we can reconstruct all the prestack datasets in CO gathers. Similarly, other seismic configurations gather, such as common-shot, can also be reconstructed. Note that the partial CRS stack, the operator size or aperture can define the degree of enhancement of the reconstructed seismic signal.

CRS-Based Denoising

We define CRS-Denoising as a process that enhances coherent seismic events, which provide information on geological structures, and attenuates random noise of prestack seismic data.

To apply CRS-based denoising, the same algorithm presented in the previous section for CRS-based interpolation and regularization can be used. The only difference is the input data, which is different in both processes. For CRS-based denoising, the input data must be previously regularized, i.e. it needs to have regular spatial sampling, without traces and stray shots.

Combination of Fourier and CRS-based Reconstruction Methods

Determining the precise CRS attributes is critical to guaranteeing the quality of the results obtained by applying these attributes and the CRS operator to seismic reflection problems, such as seismic stacking, seismic migration, data interpolation, etc. However, if the prestack input data has large gaps or very sparse sampling, the CRS attributes can be inaccurate and noisy, even when using global optimization to search for these attributes. This can lead to artifacts such as false coherent events and problems with the continuity of events in interpolated and regularized data.

In order to overcome the shortcomings of interpolation based on the CRS method, in this work we propose combining this method with interpolation based on the Fourier transform, which is the standard for processing seismic reflection data. Specifically, we propose the use of Fourier interpolation to interpolate and regularize the input prestack seismic data for the CRS method. We adopted the nome “original data" to designate pre-processed data before the regularization and interpolation stage.

Fourier+CRS Interpolation Workflow

The traditional CRS-based interpolation strategy uses only the original prestack data, both to determine the three CRS attributes and to apply the interpolation process. This workflow proposes to apply the attribute search in the reconstructed data Fourier-based Bezerra *et al.* (2022).

Below are the main steps of this workflow:

1. Applies a Fourier-based reconstruction algorithm to interpolate and regularize the original prestack data.
2. Determination of the three CRS attributes from the Fourier-based reconstructed prestack data.
3. Interpolation of the original prestack data using the three enhanced CRS attributes obtained in step 2 by the CRS partial stacking operator.

Fourier+CRS Denoising Workflow

This second workflow proposes to use the accurate attributes obtained in step 2 of the previous workflow and the CRS partial stacking operator to denoising from the prestack data reconstructed using a Fourier based method (Bezerra *et al.*, 2021). In other words, instead of applying interpolation to the original prestack data, as in the step 3 of the previous workflow, in this work we propose to apply the CRS-based interpolation to the reconstructed prestack datasets by the Fourier-based interpolation algorithms MWNI and MPFI.

Because the input data for applying the CRS-based interpolation algorithm is already interpolated and regularized, this process is called CRS-based denoising.

In the following section, we show the results of applying the proposed workflows to real data of a seismic line from the Tacutu basin. Initially, we applied the Fourier-based interpolation algorithms (MWNI and MPFI) and the CRS-based interpolation individually. We then compared the results of applying the proposed workflows, i.e. using the data reconstructed by the MWNI and MPFI algorithms as input data for the CRS interpolation method.

RESULTS AND DISCUSSIONS

In this section, we present the results using the Fourier-based reconstruction algorithms, MWNI and MPFI, to precondition the search for the wavefront CRS attributes that determine the interpolation quality, that is, random noise removal and improvement in the continuity of events of the algorithm based on partial CRS stacking. In this case, the objective is to study how the possible combinations of these algorithms with two different workflows can handle the seismic data reconstruction with large gaps (lack of shots) and sparse sampling intervals (large distances between shots and traces), in the presence of diving events and severe contamination by random noise present in 2D seismic data from Brazilian terrestrial basins.

The minimum and maximum frequencies used to Fourier-based reconstruction algorithms are, $f_{min} = 5$ and $f_{max} = 75$ Hz, respectively. In fact, most reflection seismic data have their frequency content close to these values. However, these are not optimal values for any seismic survey or different types of data. The results of the new combination strategies are compared with the results of the respective algorithms separately. We adopted PSTM migration as the main result to assess the reconstruction quality of all algorithms. We also used the RMSE and SNR metrics to evaluate the results quantitatively.

The Signal-to-Noise Ratio (SNR) is calculated as follows

$$SNR = 10 \log_{10} \left(\frac{\|\mathbf{d}\|_2^2}{\|\mathbf{d} - \hat{\mathbf{d}}\|_2^2} \right), \tag{1}$$

where $\mathbf{d}$ binning prestack data and $\hat{\mathbf{d}}$ represents the interpolated prestack data by the MWNI, MPFI and CRS algorithms. We also calculate the Relative Mean square Error (RMSE) using

$$RMSE = \frac{\|\mathbf{d} - \hat{\mathbf{d}}\|_2^2}{\|\mathbf{d}\|_2^2}. \tag{2}$$

For the application examples in seismic data presented in this work, we used codes from the three reconstruction algorithms written in MATLAB and FORTRAN and parallelized to use 40 cores of a computer with two processors of 2.60 GHz and 256 Gigabytes of RAM memory.

Tacutu Basin Data

The dataset is the seismic line 050-RL-090 of a land survey carried out in the Tacutu onshore basin, northern Brazil. The acquisition array is asymmetrical split-spread with minimum and maximum source-receiver offset of 150 and 2500 meters, respectively, each shot arrays with 96 receivers stations. The nominal intervals between sources and receivers are 200 and 50 meters, respectively. The recording time is 4 *s* with a sampling interval of 4 *ms*. Table 1 shows the acquisition parameters used to record the seismic line data. Figure 1 shows the source-receiver coordinate distribution of the original data, where black squares indicate available data and white areas inside the diagonal column indicate missing data. This data has poor quality and a low nominal fold of 12 traces per CMP. Figure 2(a) shows the common-shots gathers of three consecutive shots extracted from the original data (or pre-processed), where the central shot is missing. The data quality is poor and has a low SNR, where reflection events are blurred and obscured by noise.

Table 1. Acquisition parameters for Tacutu data line 050-RL-090.

Parameter	Value
Acquisition Year	1981
Source type	Explosive
Time Sample	4 *ms*
Record Length	4 *s*
Total Shot Point	170
Number of Channels	96
Total Station Points	8500
Total Traces	15489
Station Interval	50 m
Shot-point Interval	200 m
Spread Geometry	2500–150–0–150–2500 m
Line Extension	42200 m

The following processing flow was applied before interpolation and regularization process in the data used in this study: 1) geometry; 2) trace editing; 3) field static corrections; 4) spherical divergence com-

pensation; 5) coherent noise attenuation; 6) deconvolution; 7) velocity analysis, and 8) residual static correction. As mentioned before, the data resulting from this pre-processing is called the original data. Before using Fourier-based reconstruction, the NMO correction is applied to the data to minimize curvature in the offset axis coordinate (Trad, 2014). It is worth noting that the CRS operator does not require NMO correction or spatial windowing of the data.

The MWNI and MPFI reconstruction methods was applied in shot-receiver coordinates. The choice of these reconstruction coordinates for the Fourier-based interpolation is due to the low fold in the CMPs. The data were split into seven (7) spatial windows to ensure a better quality of Fourier-based interpolation algorithms. The total number of live shots and missing shots (in parentheses) in each window are 30(2), 23(1), 25(2), 27(5), 25(0), 26(3) and 30(3), respectively. Totalling 170 shots present, where it is desired to interpolate for a geometry with 186 shots. The data regularly sampled must have 101 receiver stations. Starting from 15489 live traces, on the parameters already defined, arrive at 18786 traces. Table 2 summarizes information about the acquisition geometries of the original and regularized data. The Fourier support (wavenumbers vector size) used in the inversion consists of 512 coefficients in each spatial dimension for each spatial window. The number of iterations used by Fourier-based methods are IRLS = 3 and CG = 10 for MWNI and it_{max} = 512 for MPFI. After interpolation, all the parts were put together to form the reconstructed prestack data.

Table 2. Original and regularized geometries of the 050-RL-090 seismic line for the 2D data of the Tacutu basin.

Data	Original	Regularized
Shot Number	170	186
Traces per Shot	96	101
Total Traces	15489	18786
Percentage (%)	82.4	100

Figures 2(b, c and d) show the common-shot gathers of the data reconstructed by the MWNI, MPFI and CRS algorithms, respectively, with the same three shots presented in Figure 2(a). The center shot and missing traces have been reconstructed, but common-shot gathers of the MWNI and MPFI algorithms

(Fig. 2(b and c)) show only a small improvement in quality, where reflection events are partially visible but not it has good continuity. We also apply to the Tacutu data the standard interpolation strategy based on CRS partial stacking, which uses the wavefront attributes extracted from the original data.

The CRS result (Fig. 2(d)) shows a significant improvement, where the reflection events appear surprisingly resolved and with strong amplitudes. In general, an improvement in the signal-to-noise ratio is perceived, which is corroborated by the SNR metric, which obtained a value of 6.73. However, we can also observe some noise in the reconstructed shot gathers, blurring the shallow events (between 0 and 0.5 *s*) and as small linear events with different dips (between black arrows). The MWNI, MPFI and CRS-based reconstruction algorithms interpolated the missed traces and shots, but as we observed, the MWNI and MPFI offers lower quality results than the CRS-based interpolation and it has some noise and artifacts.

To mitigate these noises and artifacts, we apply the first workflow (Fourier+CRS Interpolation). We use the same global optimization algorithm tuning to search for CRS attributes and the same CRS processing parameters used for regularization and interpolation application of the standard CRS workflow (Fig. 2(d)). We emphasize that the input data to search the enhanced CRS attributes is produced from the MWNI or MPFI algorithms, but interpolation based on partial CRS stacking was applied to the original prestack data using their respective accurate CRS attributes.

Figures 3(a and b) show the common-shot gathers of the data reconstructed by the first workflow based on partial CRS stacking, using the data reconstructed by the algorithms MWNI (MWNI + attributes + CRS) and MPFI (MPFI + attributes + CRS), respectively. It is possible to notice a small improvement in the whole section, such as the continuity and coherence of events and the reduction of random noise, mainly with the noise attenuation that obscured the shallow events (between 0 and 0.5 *s*). But it is still possible to identify the linear noise in the central part.

To attenuate this residual linear noise and other small artifacts, such as false events, present in the results of the first workflow, we apply the second workflow (Fourier+CRS Den oising). We emphasize that in the second proposed strategy based on partial CRS stacking, the data used to search for improved CRS attributes are the data reconstructed by the MWNI and MPFI algorithms, exactly as in the first workflow. But

these enhanced CRS attributes are applied to remove noise from the same reconstructed data (MWNI and MPFI) by applying CRS partial stacking operator to data with regular geometry, i.e. as a kind of denoising. Figures 3(c and d) show the common-shot gathers of the reconstructed data by the second workflow based on CRS partial stacking, using the data reconstructed by the MWNI (MWNI + CRS) and MPFI (MPFI + CRS) algorithms, respectively. It is possible to notice a significant improvement in the continuity of surface reflections (between 0 and 0.5 *s*), but mainly in the attenuation of the linear noise in the central part, which was practically completely removed.

Table 3 presents the RMSE and SNR metrics for the results present in the common-shot gathers for each individually tested algorithm and for the two workflows. The values of both metrics are consistent with the image analysis of the results, with a small divergence in relation to the standard application of CRS partial stacking (CRS in the table), which appears in a small advantage in relation to the results of the first workflow (MWNI/MPFI + CRS Interpolation). However, the metrics corroborate that the best results are those of the second workflow (MWNI/MPFI + CRS Denoising), with a significant advantage. This is noticeable in the Figures 3(c and d) in relation to the others results, notably as small contamination by random and linear noise and better continuity and coherence of events.

Table 3. RMSE and SNR values for all algorithms and workflows tested on the Tacutu data.

Algorithm/Workflows	RMSE (%)	SNR (db)
MWNI	807.96	2.06
MPFI	687.95	2.27
CRS	448.23	6.73
MWNI + CRS Interpolation	451.35	6.55
MPFI + CRS Interpolation	470.78	6.52
MWNI + CRS Denoising	**160.73**	**9.07**
MPFI + CRS Denoising	168.47	8.38

In Figures 4 we compare the coherence attribute extracted from the original data with those extracted from the reconstructed data by the MWNI and MPFI algorithms. Figure 4(a) corresponds to the coherence of the original data, and shows erroneous high values at the top of the section (between 0 and 0.2 *s*) that are related to noise caused by shot gaps and missing traces. Figure 4(b) shows the coherence obtained

from the data regularized by the MWNI algorithm, where its values are more consistent and shows a significant improvement of the coherent events in the inclined part. Figure 4(c) shows the coherence section obtained from the data reconstructed by the MPFI algorithm, showing a significant noise removal and improvement of shallow events (between 0 and 0.2 *s*). This result is similar to that obtained from the data reconstructed by the MWNI algorithm (Fig. 4(b)), with a slight advantage for the MWNI.

In Figures 5 we compare the emergence angle attribute extracted from the original data with those extracted from the reconstructed data by the MWNI and MPFI algorithms. Figure 5(a) presents the emergence angle extracted from the original data, where it is possible to perceive a greater discontinuity of events and a greater prevalence of noise (between 0 and 0.6 *s*). This noise has been greatly attenuated and the continuity of events has improved dramatically in Figure 5(b), which presents the emergence angle extracted from the data regularized by the MWNI algorithm. Figure 5(c) shows the emergence angle section obtained from the data reconstructed by the MPFI algorithm, where a significant noise reduction and improvement in the continuity of events is observed in relation to the original data. These result is similar to that obtained from the data reconstructed by the MWNI algorithm (Fig. 5(b)), with a significant advantage for the MWNI, mainly in the shallow part (between 0 and 0.6 *s*) and curved events.

In Figures 6 we compare the radius of curvature of the NIP wave (Rnip) attribute extracted from the original data with those extracted from the reconstructed data by the MWNI and MPFI algorithms. Figure 6(a) presents the Rnip extracted from the original data, being perceptible the discontinuity of the events caused by the strong prevalence of noise, mainly by linear noise in all section. The Rnip extracted from the MWNI reconstructed data (Fig. 6(b)) is smoother than the curvature extracted from the original data (Fig. 6(a)). The former presents better lateral continuity and less contamination by linear noise. We can say the same for Figure 6(c) where we present the Rnip section obtained from the data reconstructed by the MPFI algorithm. These result is similar to that obtained from the data reconstructed by the MWNI algorithm (Fig. 6(b)), with a significant advantage for the MWNI, mainly regarding linear noise and events smoothness. We do not show the attribute of the radius of curvature of the normal wave (Rn) due to the difficulty in perceiving the differences.

The variation of the CRS attributes between events has to be smooth because the CRS operator is an approximation of paraxial ray theory, which is valid for smoothly heterogeneous media. Due to this fact, any strong non-physical fluctuation or due to spurious events must be corrected. The CRS attributes obtained from the reconstructed MWNI and MPFI data are smoother and have less anomalous fluctuations, so are more suitable for applications.

The preconditioning of the original data performed by the MWNI and MPFI algorithms was effective, i.e. they proposed interpolated and regularized prestack data, with a slight enhancement of the events and noise attenuation. The preconditioning performed by the MWNI algorithm was more successful in this case, due to its ability to preserve amplitude, even in the presence of inclined events, where the MPFI algorithm needs to use many iterations. The truncation in 512 iterations, impaired the preservation of events by the MPFI in parts of the data. It ended up resulting in a lower reconstruction quality of the CRS partial stacking application. However, we emphasize that the result is better than the standard application of CRS. That is, any of these or similar Fourier-based methods should produce more satisfactory results than the standard CRS application.

We applied Kirchhoff prestack time migration (PSTM) to evaluate the reconstruction quality of all datasets, using the same velocity model and migration parameters for a fair comparison. Figure 7(a) shows the original data PSTM image, which, in general, is noisy and has poor continuity of reflection events. The shallow part of the image shows an intense noise, interrupting shallow reflection events. The PSTM images obtained from the data reconstructed by MWNI and MPFI algorithms (Figs. 7(b and c)), in general, also has low quality but slightly improves reflector continuity of the reflection events in the middle and deeper parts of the image. Figure 7(d) shows the PSTM image obtained from the reconstructed data by standard CRS-based interpolation workflow in the original data. As expected, this result shows significant improvement, with dramatically increased signal-to-noise ratio and improved continuity of reflection events, especially in the central and deeper parts. However, we can see that the shallow part has several problems and creates artifacts with strong amplitudes that interrupt the continuity of shallow reflections. This limitation happens because the CRS attributes are searched using automatic coherence analysis,

which allows the inclusion of false coherent events.

Figures 7(e and g) show the migrated PSTM sections obtained from the reconstructed data by the first workflow for the MWNI (MWNI + attributes + CRS) and MPFI (MPFI + attributes + CRS) algorithms, respectively. We can observe a strong improvement in the continuity of the shallow reflectors and a reduction in linear artifacts in relation to the standard CRS application (Fig. 7(d)). These results are similar to each other, with a slight advantage for MWNI preconditioning (Fig. 7(e)). Figures 7(f and h) show the migrated PSTM images obtained from the reconstructed data by the second workflow for the MWNI (MWNI + CRS) and MPFI (MPFI + CRS) algorithms, respectively. They are cleaner and have higher quality because the continuity of the reflectors has been better resolved, even in the shallowest parts and the artifacts and migration noise was also greatly attenuated. These results also are similar to each other, with a slight advantage for MWNI preconditioning (Fig. 7(f)).

CONCLUSIONS

We present the successful combination of two classes of interpolation methods, the well-known Fourier-based interpolation algorithms MWNI and MPFI, and the CRS-based interpolation, applied to 2D land seismic data.

Through applications to data from the Tacutu basin, we show that the independent application of each method does not produce satisfactory results. The MWNI and MPFI methods slightly improves the quality of the regularized data and also of the migrated images. Interpolation based on the standard CRS operator workflow produces results with a high signal-to-noise ratio and improved reflections, but creates spurious or noisy events that contaminate the migrated image and destroy continuity, especially for near-surface or shallow events.

To solve the shortcomings of the CRS-based data reconstruction, we apply the search for CRS attributes in the prestack data reconstructed by the MWNI and MPFI methods. The improved CRS attributes present significant differences in relation to the original ones, they are smoother and most of the non-physical fluctuations have been removed, presenting a better quality and accuracy for applications in seismic reflection problems. The application in land data from the Tacutu basin of these approaches, combining the interpolation methods, provides high-quality results. The coherent false events were attenuated, and the artifacts caused in the migrated image have also been removed. We show that these workflows is the best alternative for reprocessing old seismic data, mainly with low quality (noise), coarse spatial sampling, and low fold.

The application of the improved CRS attributes, obtained from the reconstructed data by the MWNI and MPFI algorithms, to regularize and interpolate the original data by the CRS partial stacking operator produces a great improvement in the quality of the reconstructed data. These improvements are noticeable both in the common-shot gathers and PSTM migrated images and verified by the metrics SNR and RMSE. We also apply the CRS reconstruction method to data preconditioned data by the MWNI and MPFI algorithms, which we call denoising. The results show a significant improvement over the first strategy, with greater linear noise removal and better continuity of events, enhancing reflections. In this way, the ex-

tracted CRS attributes are smoother and less contaminated by coherent noise produced by gaps due to missed shots and traces and coarse spatial sampling.

The two workflows for combining Fourier-based and CRS-based interpolation methods provide prestack data of improved quality and without artifacts. These are an alternative to the standard processing of land data with low quality (noisy and low coverage).

The computational cost of the MWNI+CRS strategy is close to that of the standard CRS, as the CPU time of MWNI is less than 1% of the CRS. The MPFI+CRS strategy, on the other hand, has a higher computational cost, due to the MPFI having a much higher CPU time than the MWNI. The adoption of the Fast MPFI algorithm should reduce the total computational cost of the MPFI+CRS strategy, making it more competitive compared to MWNI+CRS. Since the MWNI and MPFI interpolation computational time is very low for 2D datasets, it does not significantly affect or increases the computational time spent by the CRS-based interpolation method. Future research will study the combination Fourier-based and CRS-based methods for 5D interpolation.

ACKNOWLEDGMENTS

This work was supported by the *Agência Nacional de Petróleo, Gás Natural e Biocombustíveis* (ANP) Brazil, through the Investment Clause in Research, Development, and Innovation, included in the contracts for Exploration, Development, and Production of Oil and Natural Gas.

DATA AVAILABILITY STATEMENT

Data associated with this research are confidential and cannot be released.

CONFLICT OF INTEREST

There is no conflict of interest.

REFERENCES

Abma, R.; Kabir, N. 3D interpolation of irregular data with a POCS algorithm. *GEOPHYSICS* **2006**, *71*, E91–E97. 10.1190/1.2356088.

Baykulov, M.; Gajewski, D. Prestack seismic data enhancement with partial common-reflection-surface (CRS) stack. *GEOPHYSICS* **2009**, *74*, V49–V58. 10.1190/1.3106182.

Bezerra, Y.S.F.; Garabito, G.; Sacchi, M. Preconditioning of 2D land seismic data using a combination of MPFI and CRS methods. Proceeding of the 17th International Congress of the Brazilian Geophysical. Brazilian Geophysical Society, 2021. 10.22564/17cisbgf2021.270.

Bezerra, Y.S.; Garabito, G.; Sacchi, M.D.; Caldeira, J.L. Data reconstruction combining MWNI and CRS-based interpolation methods. *Journal of Applied Geophysics* **2022**, *19X*, 104445. 10.1016/j.jappgeo.2022.

Chiu, S.K. Multidimensional interpolation using a model-constrained minimum weighted norm interpolation. *GEOPHYSICS* **2014**, *79*, V191–V199. 10.1190/geo2014-0086.1.

Garabito, G.; Stoffa, P.L.; Lucena, L.S.; Cruz, J.C. Part I — CRS stack: Global optimization of the 2D CRS-attributes. *Journal of Applied Geophysics* **2012**, *85*, 92–101. 10.1016/j.jappgeo.2012.07.005.

Garabito, G.; Stoffa, P.L.; Bezerra, Y.S.F.; Caldeira, J.L. Combination of the common reflection surface-based prestack data regularization and reverse time migration: Application to real land data. *GEOPHYSICS* **2021**, *86*, S155–S164. 10.1190/geo2020-0135.1.

Garabito, G. A comparative study of common-reflection-surface prestack time migration and data regularization: Application in crooked-line data. *GEOPHYSICS* **2018**, *83*, S355–S364. 10.1190/geo2017-0691.1.

Hoecht, G.; Ricarte, P.; Bergler, S.; Landa, E. Operator-oriented CRS interpolation. *Geophysical Prospecting* **2009**, *57*, 957–979. 10.1111/j.1365-2478.2009.00789.x.

Hunt, L.; Downton, J.; Reynolds, S.; Hadley, S.; Trad, D.; Hadley, M. The effect of interpolation on imaging and AVO: A Viking case study. *GEOPHYSICS* **2010**, *75*, WB265–WB274. 10.1190/1.3475390.

Liu, B.; Sacchi, M.D. Minimum weighted norm interpolation of seismic records. *GEOPHYSICS* **2004**,

69, 1560–1568. 10.1190/1.1836829.

Mallat, S.; Zhang, Z. Matching pursuits with time-frequency dictionaries. *IEEE Transactions on Signal Processing* **1993**, *41*, 3397–3415. 10.1109/78.258082.

Muhtar, L.K.; Triyoso, W.; Fatkhan, F. Application of common reflection surface (CRS) to velocity variation with azimuth (VVAz) inversion of the relatively narrow azimuth 3D seismic land data. *Open Physics* **2021**, *19*, 439–446. 10.1515/phys-2021-0051.

Nguyen, T.; Winnett, R. Seismic interpolation by optimally matched Fourier components. SEG Technical Program Expanded Abstracts 2011. Society of Exploration Geophysicists, 2011. 10.1190/1.3627836.

Rad, P.B.; Hickey, C.J. Using common-reflection-surface stack for enhanced near-surface seismic reflection imaging: Examples from consolidated and unconsolidated environments. *GEOPHYSICS* **2022**, *87*, EN45–EN56. 10.1190/geo2021-0437.1.

Sacchi, M.; Ulrych, T.; Walker, C. Interpolation and extrapolation using a high-resolution discrete Fourier transform. *IEEE Transactions on Signal Processing* **1998**, *46*, 31–38. 10.1109/78.651165.

Schonewille, M.A.; Romijn, R.; Duijndam, A.J.W.; Ongkiehong, L. A general reconstruction scheme for dominant azimuth 3D seismic data. *GEOPHYSICS* **2003**, *68*, 2092–2105. 10.1190/1.1635063.

Schonewille, M.; Klaedtke, A.; Vigner, A. Anti-alias anti-leakage Fourier transform. SEG Technical Program Expanded Abstracts 2009. Society of Exploration Geophysicists, 2009. 10.1190/1.3255533.

Schonewille, M.; Yan, Z.; Bayly, M.; Bisley, R. Matching pursuit Fourier interpolation using priors derived from a second data set. SEG Technical Program Expanded Abstracts 2013. Society of Exploration Geophysicists, 2013. 10.1190/segam2013-0956.1.

Schwarz, B.; Vanelle, C.; Wißmath, S.; Bauer, A.; Gajewski, D. Efficient common-reflection-surface-based prestack slope determination for stereotomography. SEG Technical Program Expanded Abstracts 2015. Society of Exploration Geophysicists, 2015. 10.1190/segam2015-5930197.1.

Soleimani, M.; Roshandel Kahoo, A. Optimizing design of 3D seismic acquisition by CRS trace interpolation. *Journal of the Earth and Space Physics* **2016**, *42*, 01–12. 10.22059/jesphys.2016.58886.

Stanton, A.; Sacchi, M.D. All roads lead to Rome: predictability, sparsity, rank and pre-stack seismic data

reconstruction. *RECORDER* **2013**, *38*, 32–37.

Trad, D. Five-dimensional interpolation: New directions and challenges. *CSEG Recorder* **2014**, pp. 40–46.

Xu, S.; Zhang, Y.; Pham, D.; Lambaré, G. Antileakage Fourier transform for seismic data regularization. *GEOPHYSICS* **2005**, *70*, V87–V95. 10.1190/1.1993713.

Zwartjes, P.; Gisolf, A. Fourier reconstruction with sparse inversion. *Geophysical Prospecting* **2007**, *55*, 199–221. 10.1111/j.1365-2478.2006.00580.x.

Zwartjes, P.M.; Sacchi, M.D. Fourier reconstruction of nonuniformly sampled, aliased seismic data. *GEOPHYSICS* **2007**, *72*, V21–V32. 10.1190/1.2399442.

FIGURES

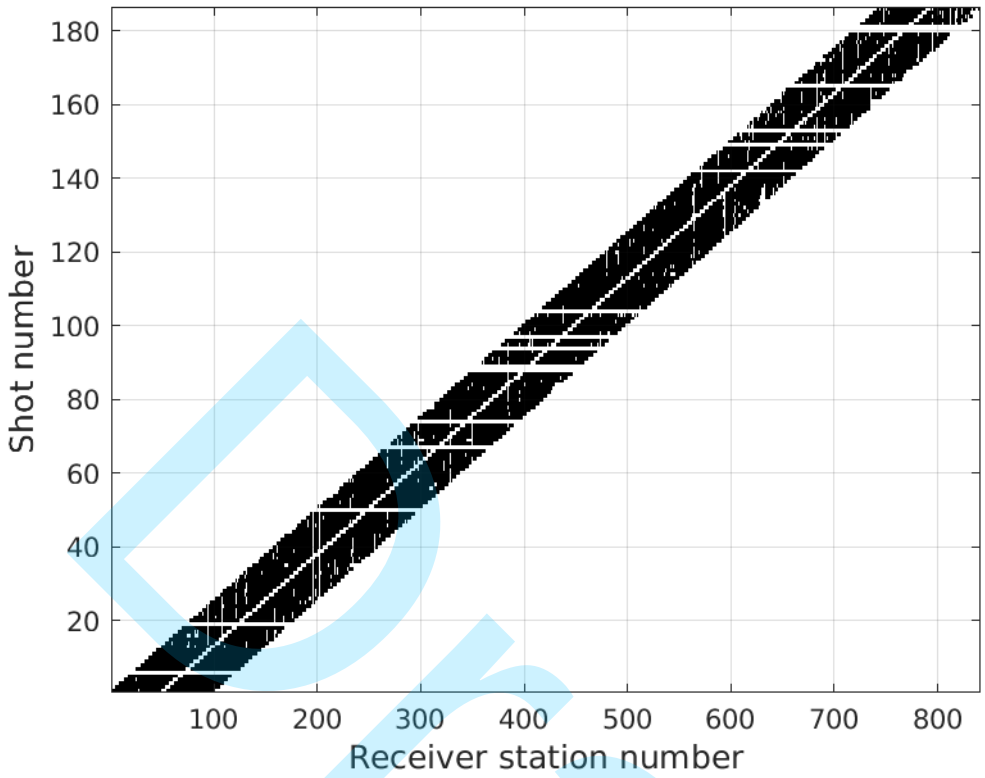

Figure 1. Shots and receivers distribution map of the Tacutu basin data. The black squares indicate available traces, and white areas within the diagonal strip indicate missing traces. The large white areas are the gaps that correspond to the missed shots.

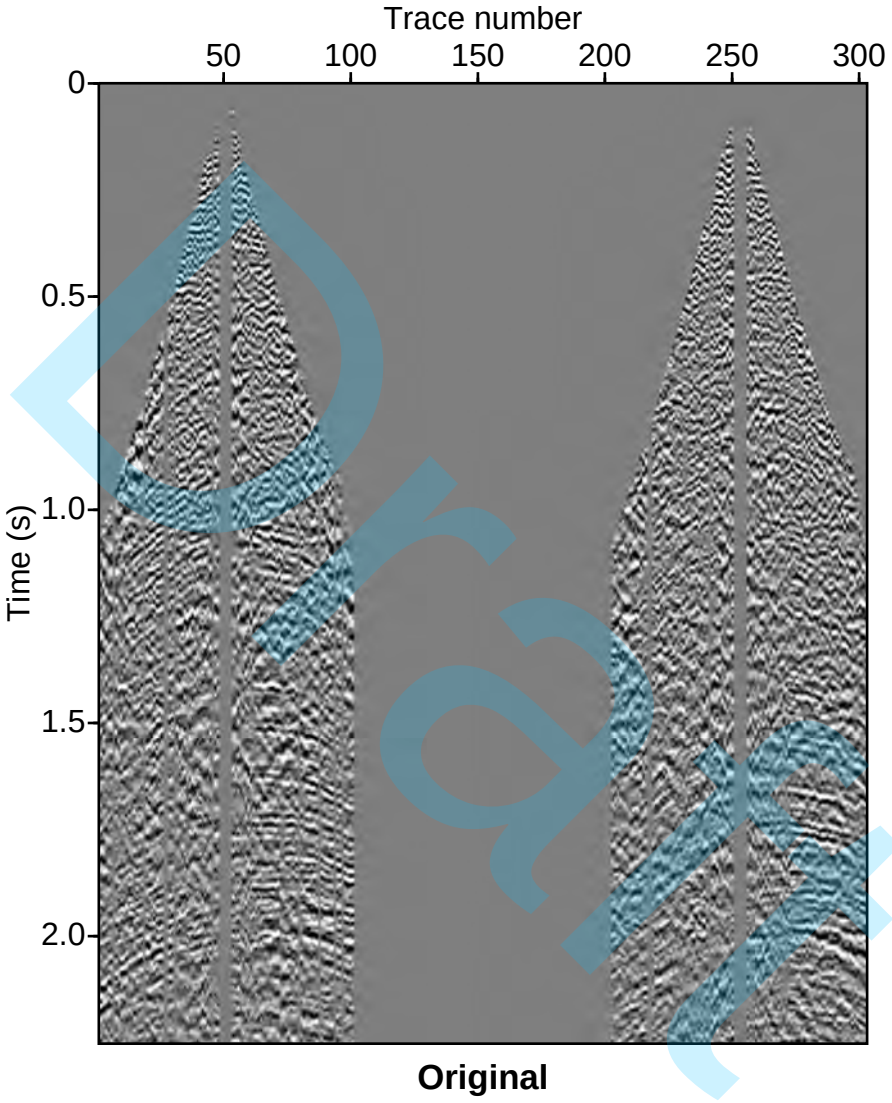

Figure 2. Common-shot gathers extracted from the original and reconstructed datasets of the Tacutu basin. a) original data, b) reconstructed data with MWNI method, c) reconstructed data with MPFI method and d) reconstructed data with the CRS-based method using the wavefront attributes extracted from the original data.

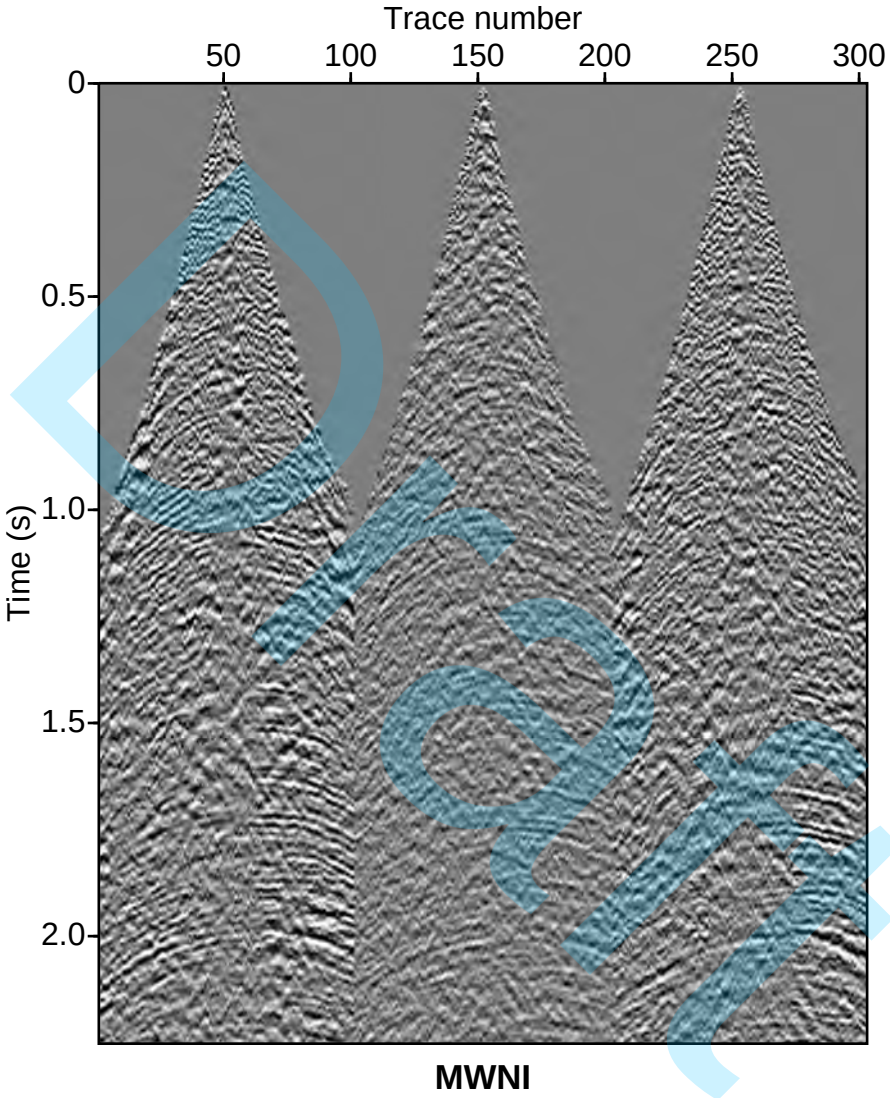

Figure 2. Common-shot gathers extracted from the original and reconstructed datasets of the Tacutu basin. a) original data, b) reconstructed data with MWNI method, c) reconstructed data with MPFI method and d) reconstructed data with the CRS-based method using the wavefront attributes extracted from the original data.

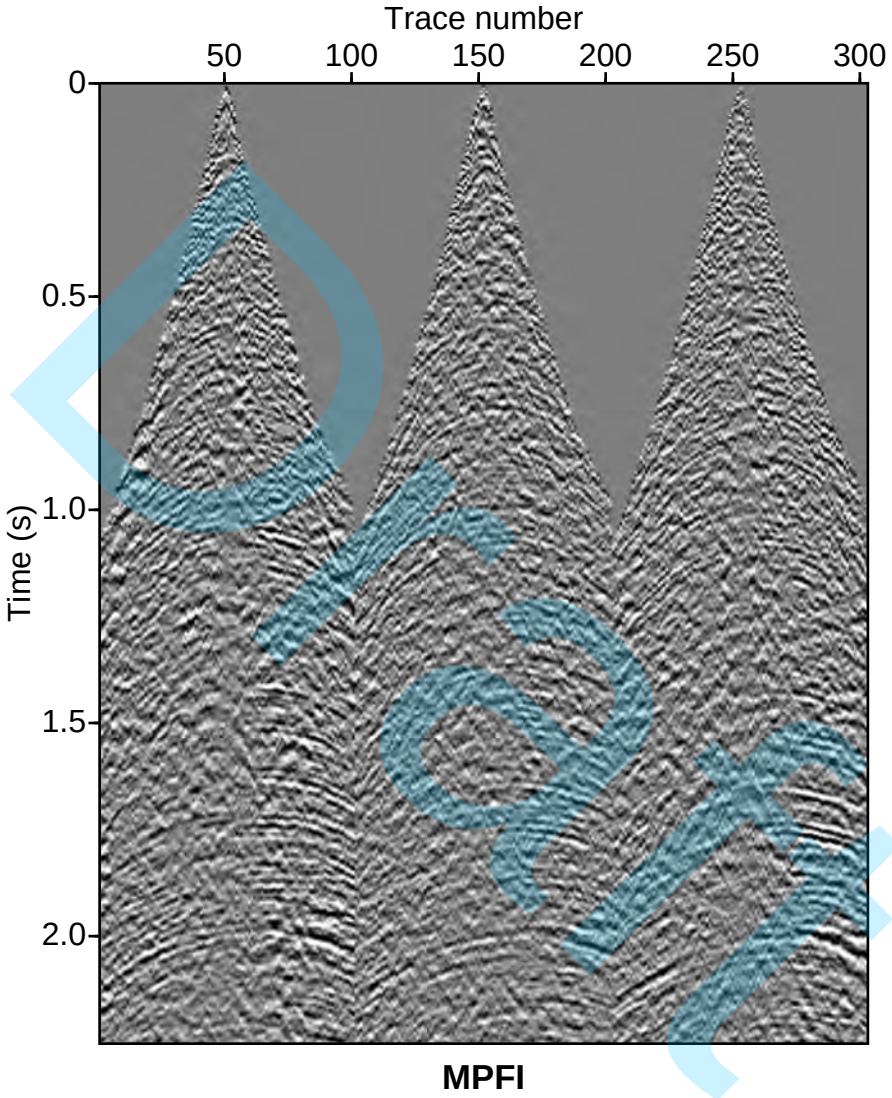

Figure 2. Common-shot gathers extracted from the original and reconstructed datasets of the Tacutu basin. a) original data, b) reconstructed data with MWNI method, c) reconstructed data with MPFI method and d) reconstructed data with the CRS-based method using the wavefront attributes extracted from the original data.

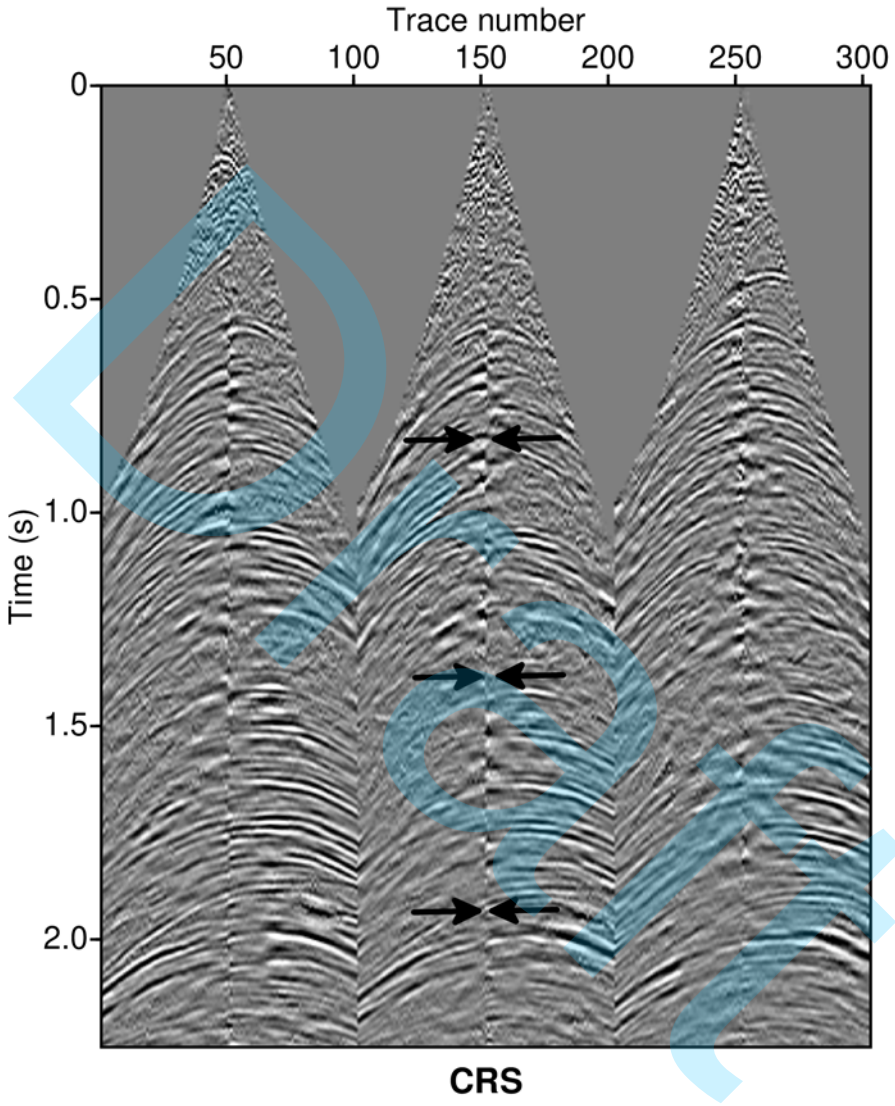

Figure 2. Common-shot gathers extracted from the original and reconstructed datasets of the Tacutu basin. a) original data, b) reconstructed data with MWNI method, c) reconstructed data with MPFI method and d) reconstructed data with the CRS-based method using the wavefront attributes extracted from the original data.

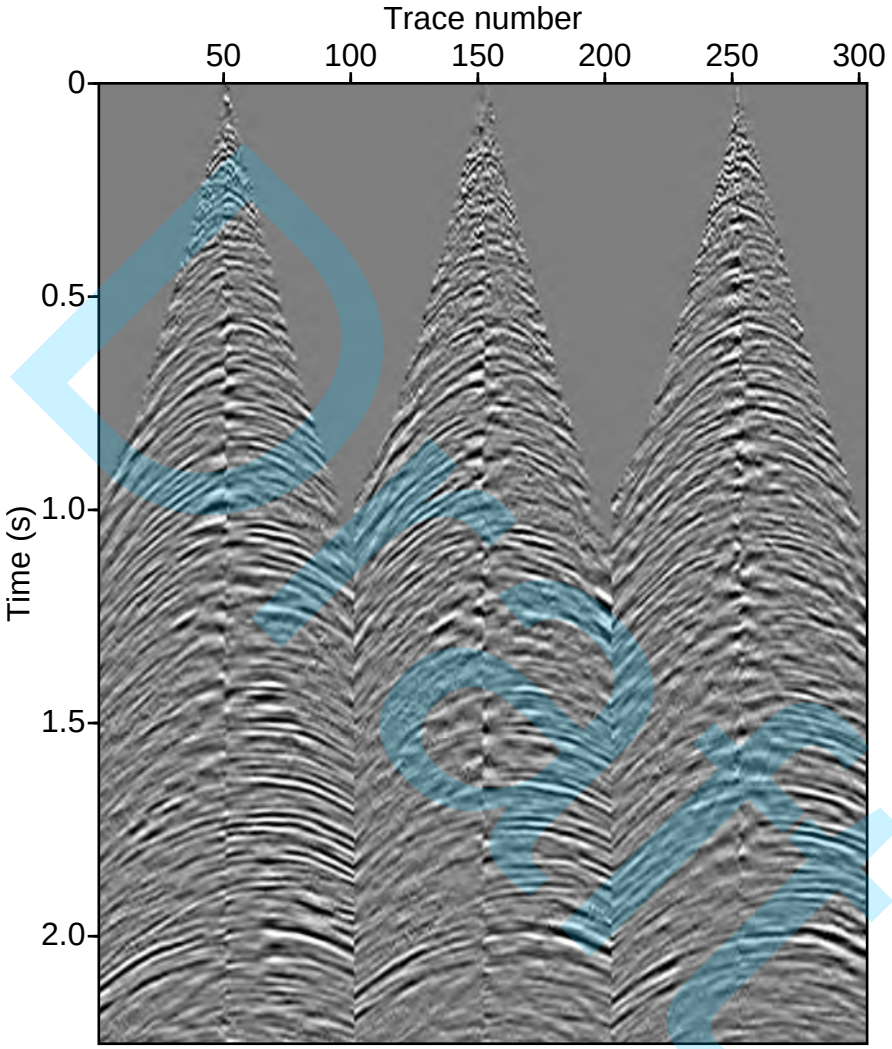

Figure 3. Common-shot gathers extracted from the original and combination Fourier+CRS reconstructed datasets of the Tacutu basin. a) MWNI + CRS Interpolation, b) MPFI + CRS Interpolation, c) MWNI + CRS Denoising and d) MPFI + CRS Denoising.

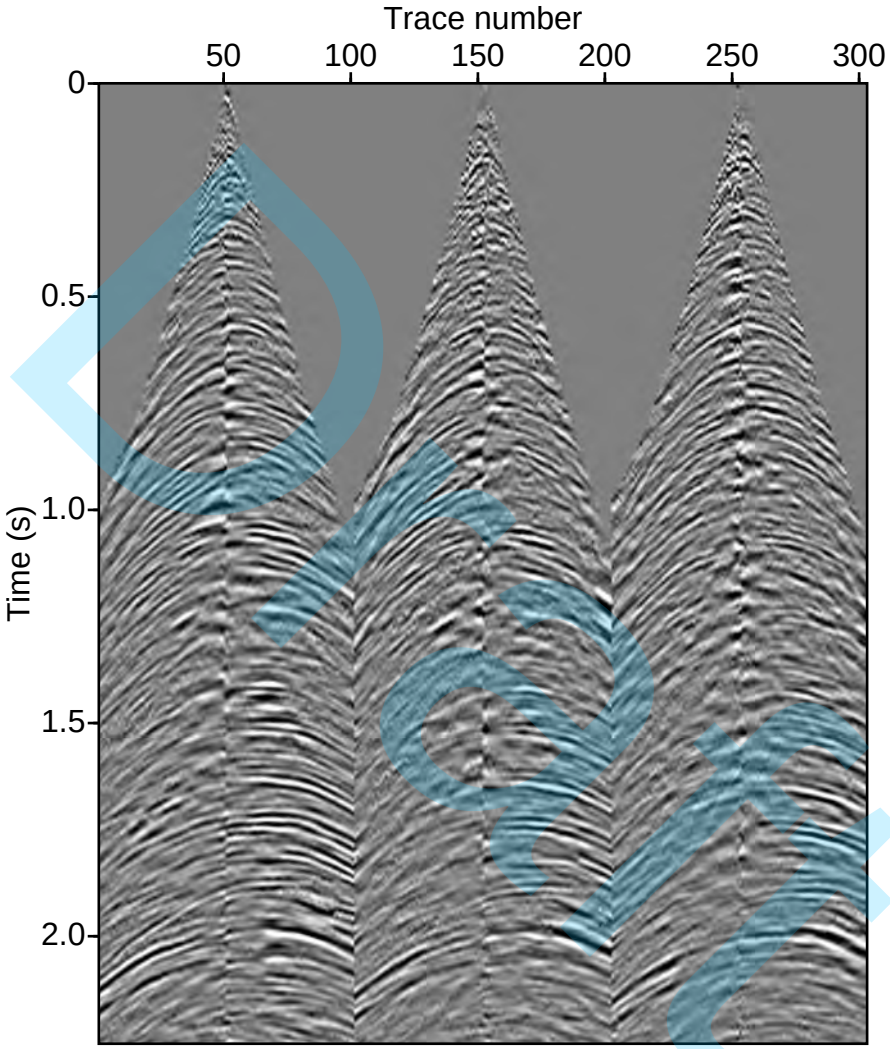

Figure 3. Common-shot gathers extracted from the original and combination Fourier+CRS reconstructed datasets of the Tacutu basin. a) MWNI + CRS Interpolation, b) MPFI + CRS Interpolation, c) MWNI + CRS Denoising and d) MPFI + CRS Denoising.

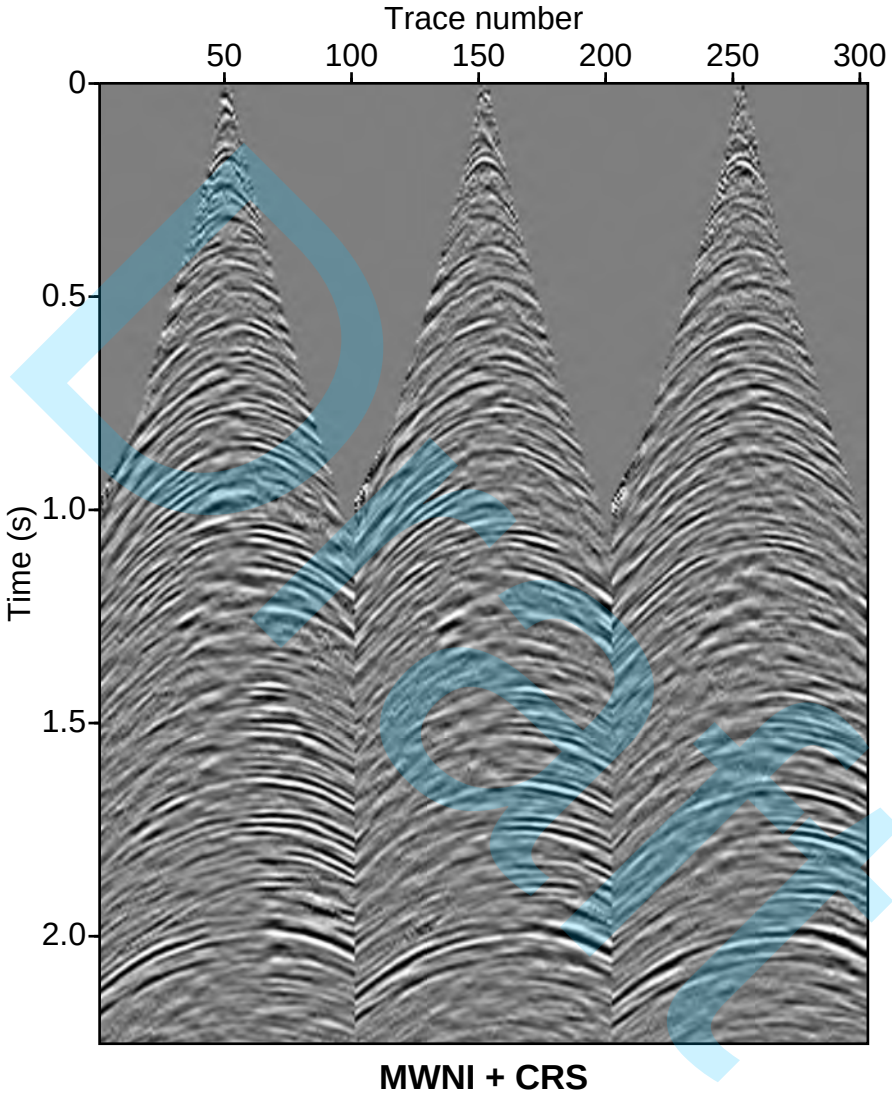

Figure 3. Common-shot gathers extracted from the original and combination Fourier+CRS reconstructed datasets of the Tacutu basin. a) MWNI + CRS Interpolation, b) MPFI + CRS Interpolation, c) MWNI + CRS Denoising and d) MPFI + CRS Denoising.

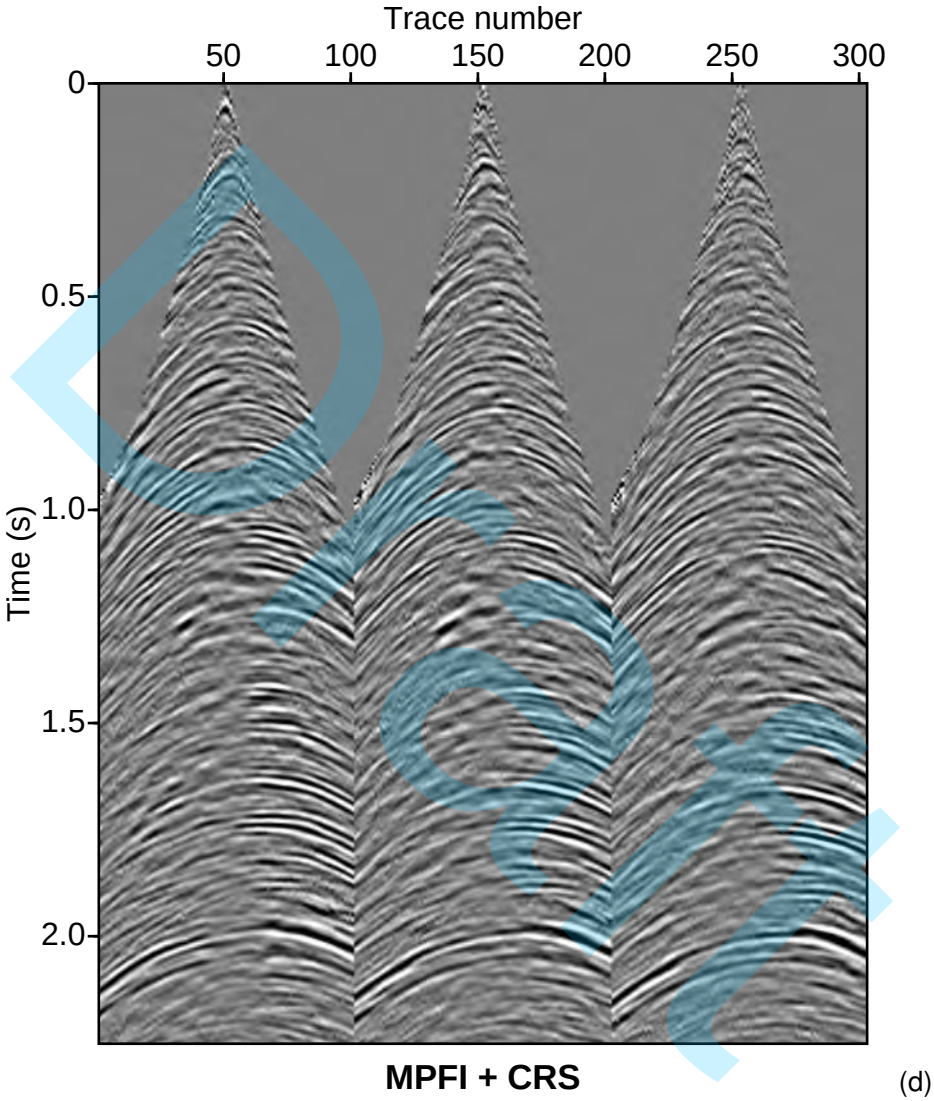

Figure 3. Common-shot gathers extracted from the original and combination Fourier+CRS reconstructed datasets of the Tacutu basin. a) MWNI + CRS Interpolation, b) MPFI + CRS Interpolation, c) MWNI + CRS Denoising and d) MPFI + CRS Denoising.

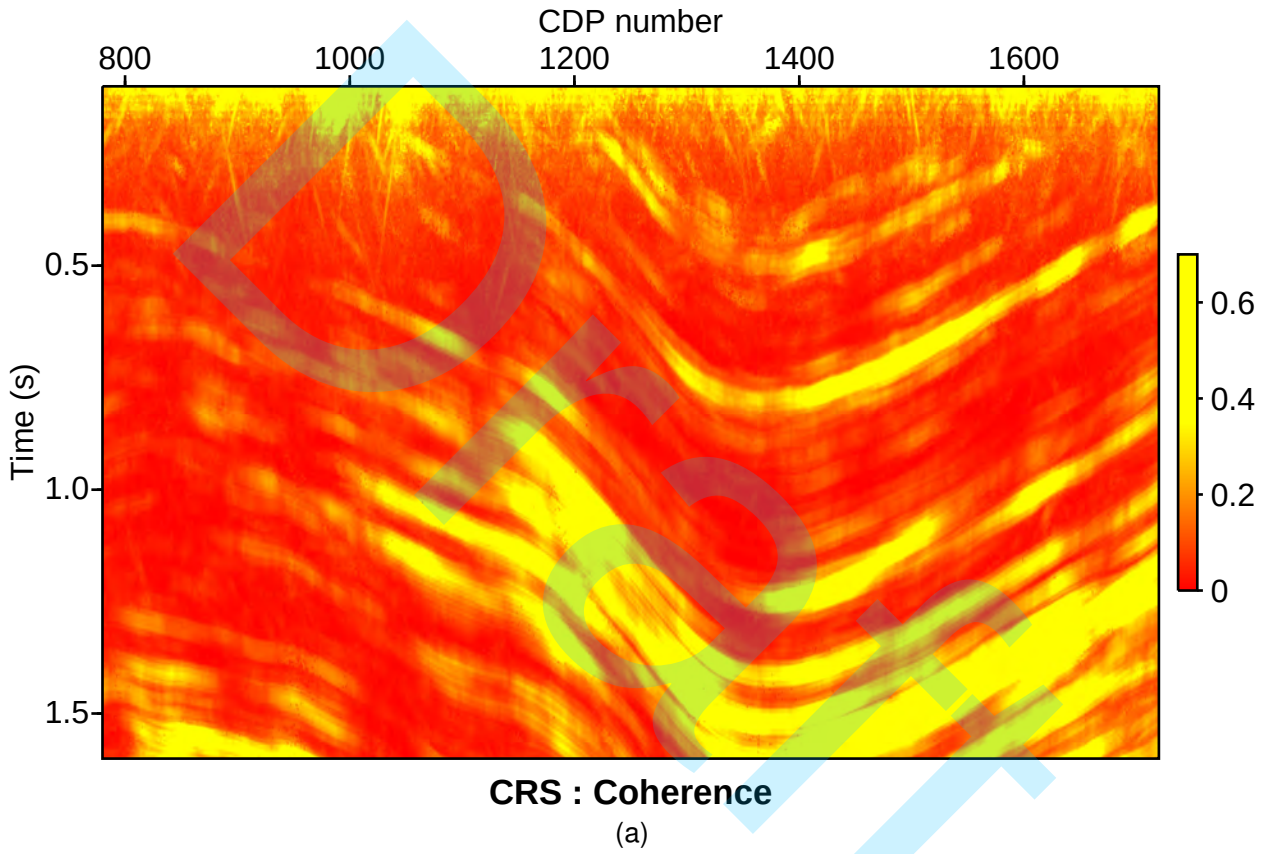

Figure 4. Coherence semblance sections from CRS attributes determined from a) original data, b) preconditioned data with MWNI method and c) preconditioned data with MPFI method. The CRS attributes obtained from the MWNI data (b) show less noise interference.

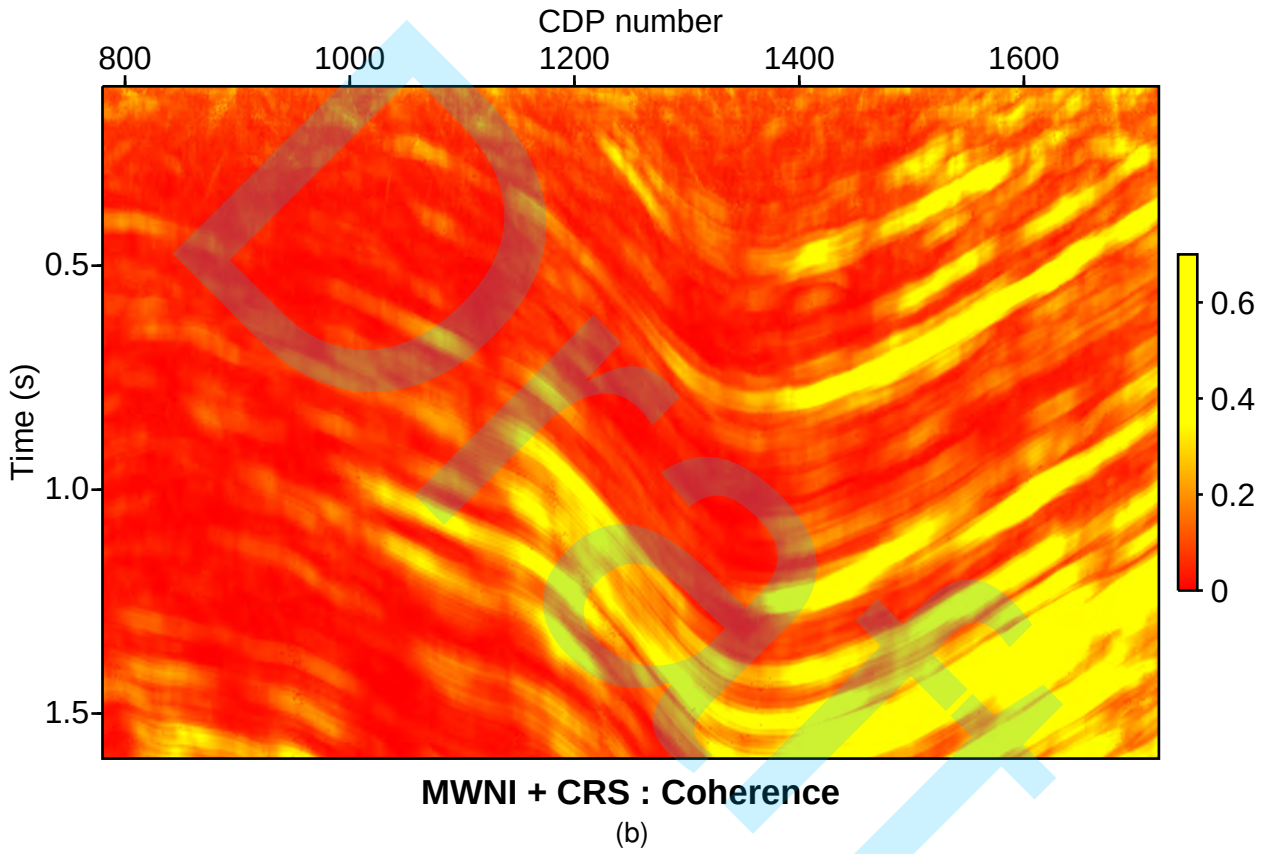

Figure 4. Coherence semblance sections from CRS attributes determined from a) original data, b) preconditioned data with MWNI method and c) preconditioned data with MPFI method. The CRS attributes obtained from the MWNI data (b) show less noise interference.

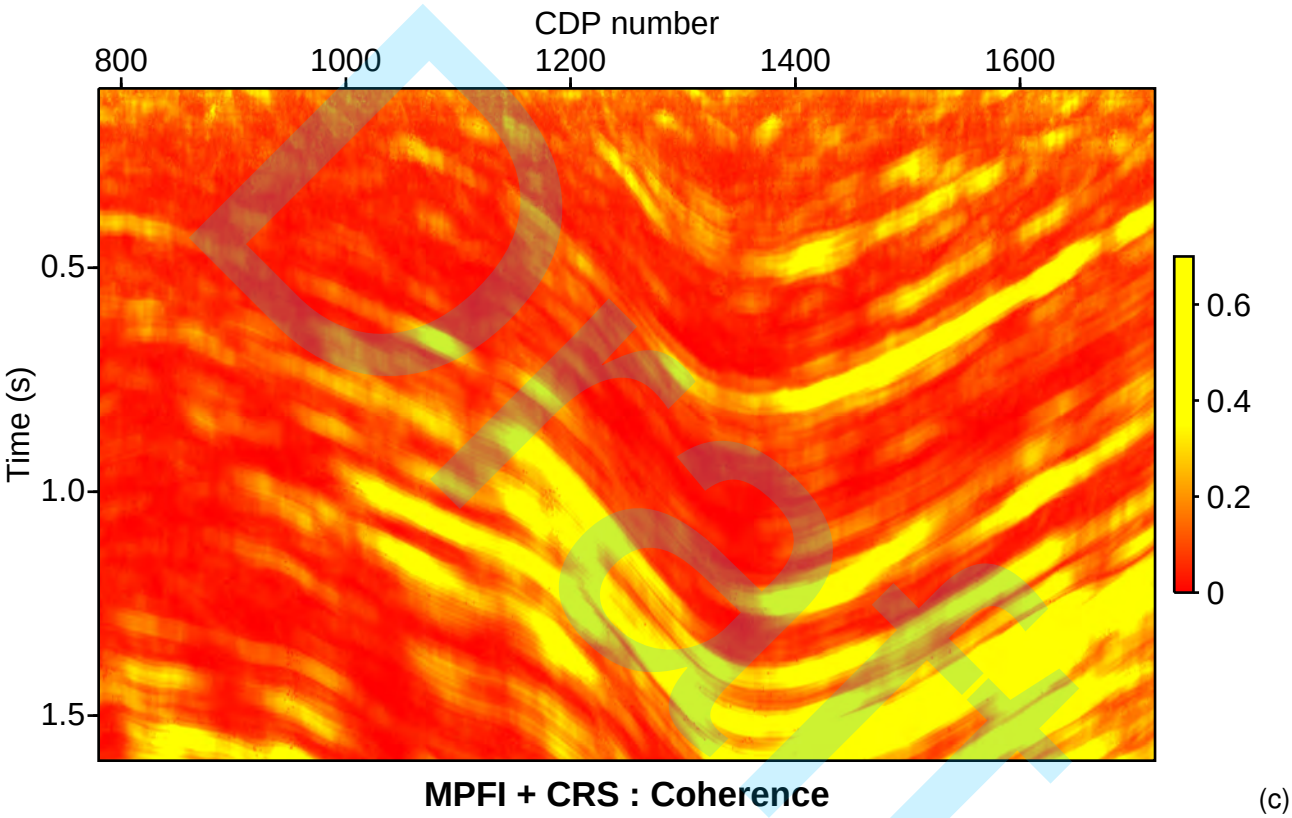

Figure 4. Coherence semblance sections from CRS attributes determined from a) original data, b) preconditioned data with MWNI method and c) preconditioned data with MPFI method. The CRS attributes obtained from the MWNI data (b) show less noise interference.

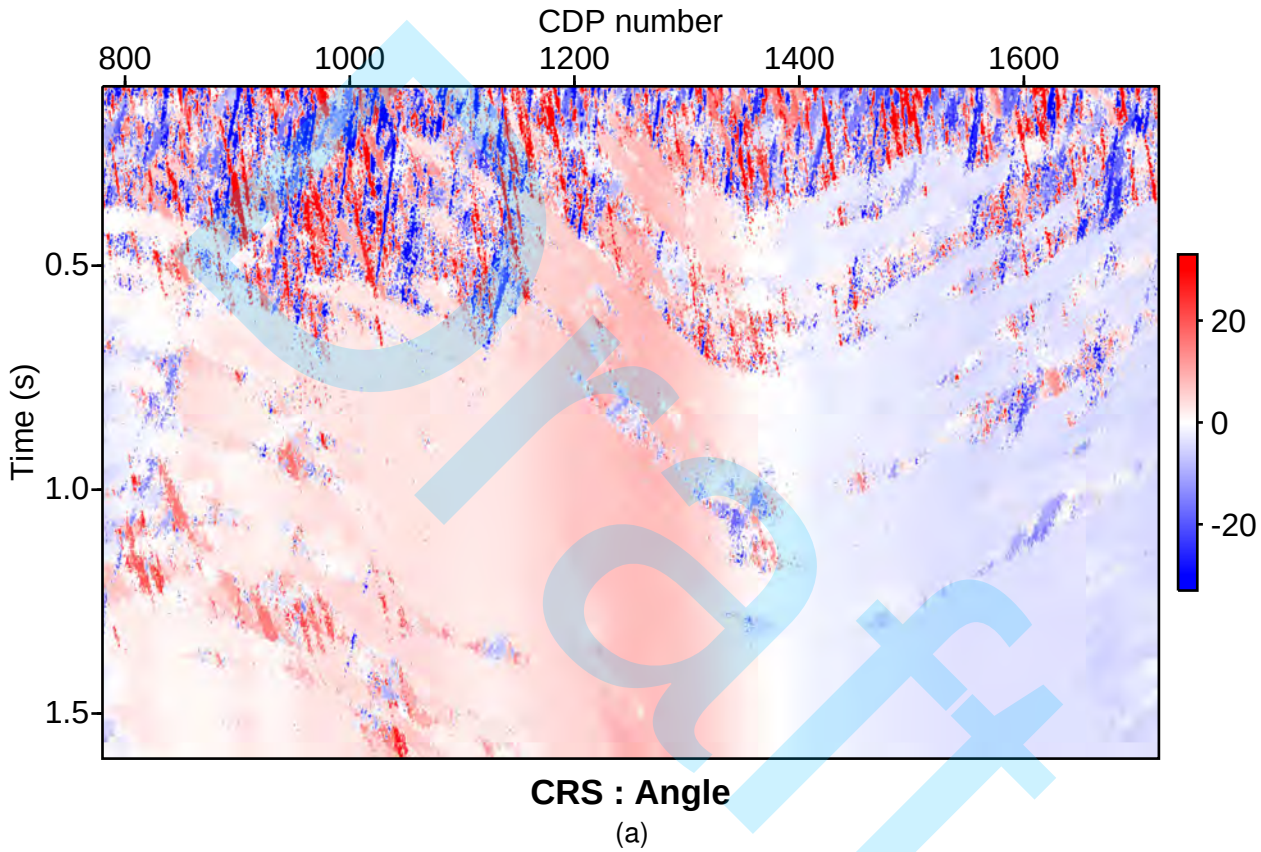

Figure 5. Emergence angle sections from CRS attributes determined from a) original data, b) preconditioned data with MWNI method and c) preconditioned data with MPFI method. The CRS attributes obtained from the MWNI data (b) show less noise interference.

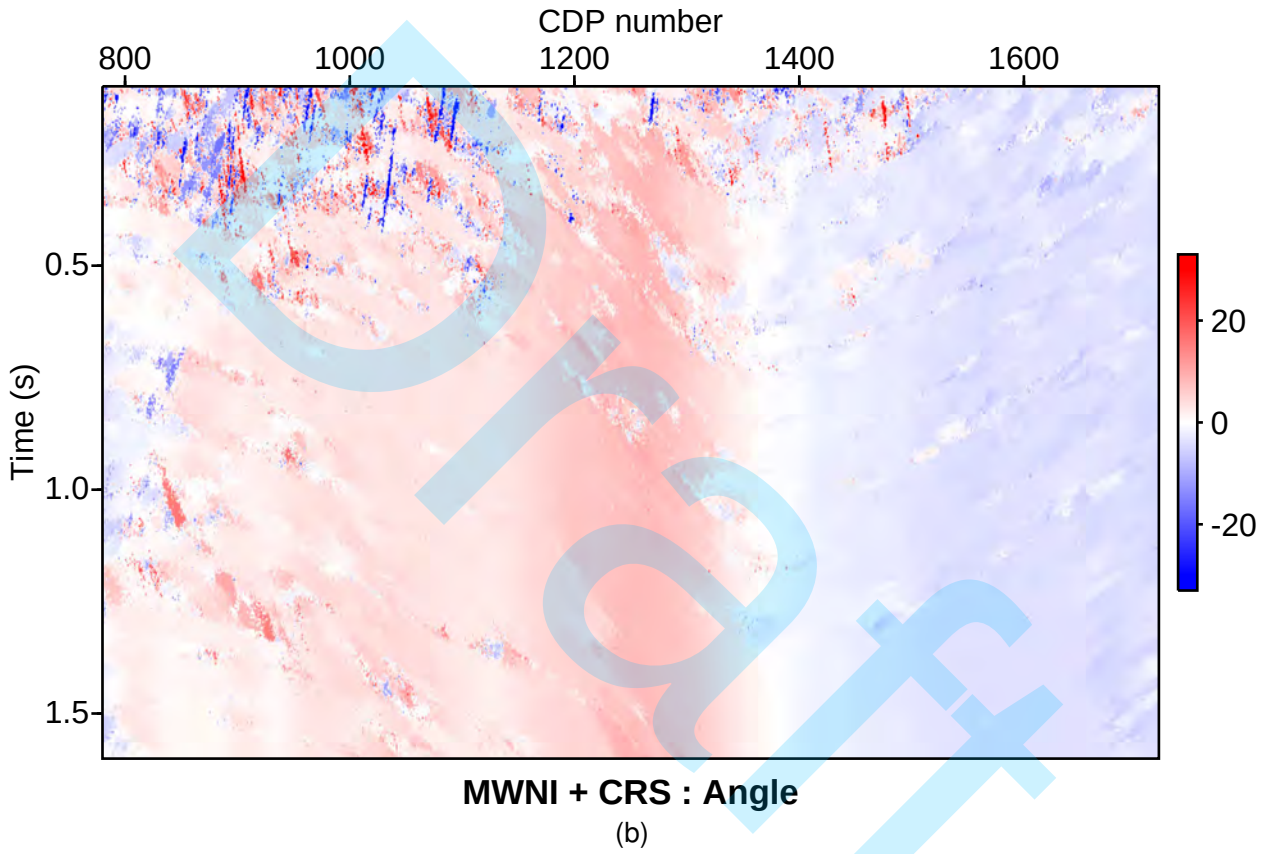

Figure 5. Emergence angle sections from CRS attributes determined from a) original data, b) preconditioned data with MWNI method and c) preconditioned data with MPFI method. The CRS attributes obtained from the MWNI data (b) show less noise interference.

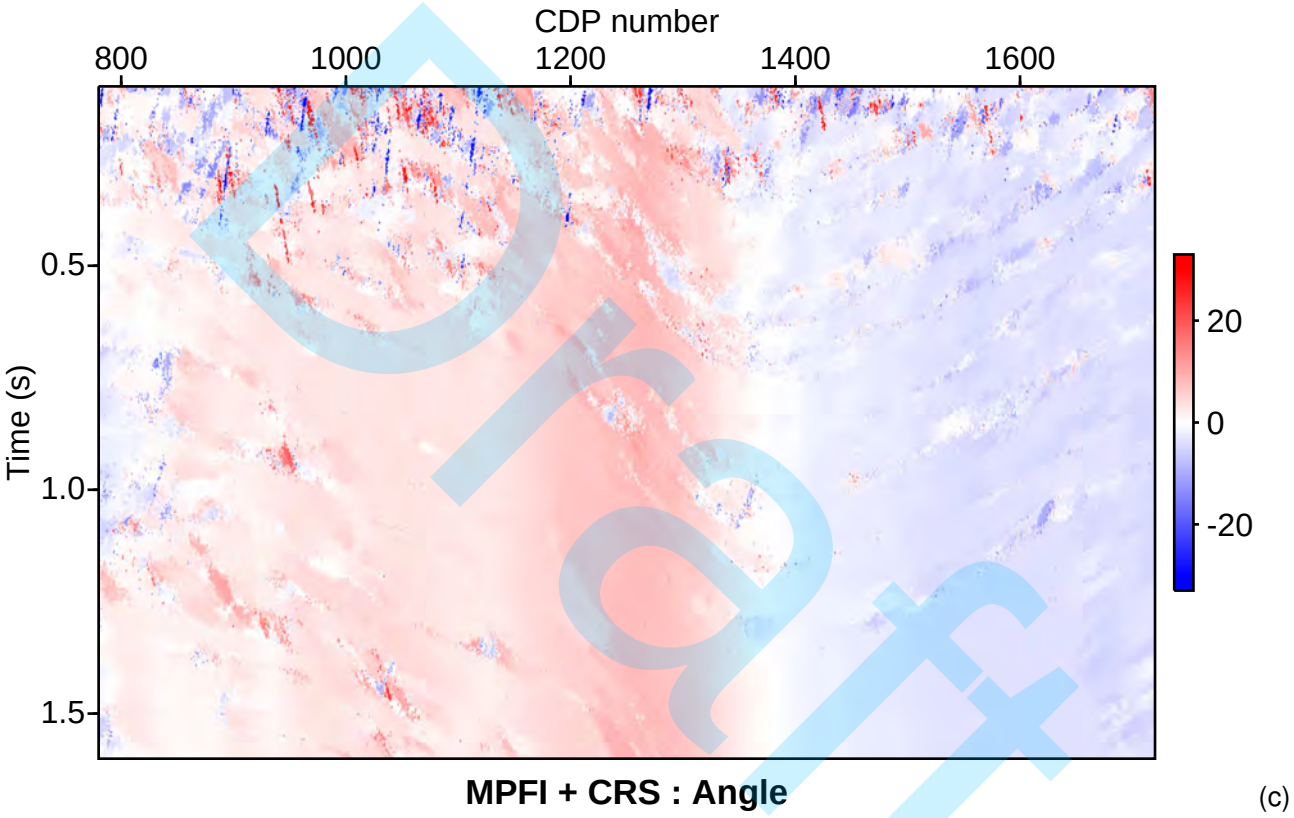

Figure 5. Emergence angle sections from CRS attributes determined from a) original data, b) preconditioned data with MWNI method and c) preconditioned data with MPFI method. The CRS attributes obtained from the MWNI data (b) show less noise interference.

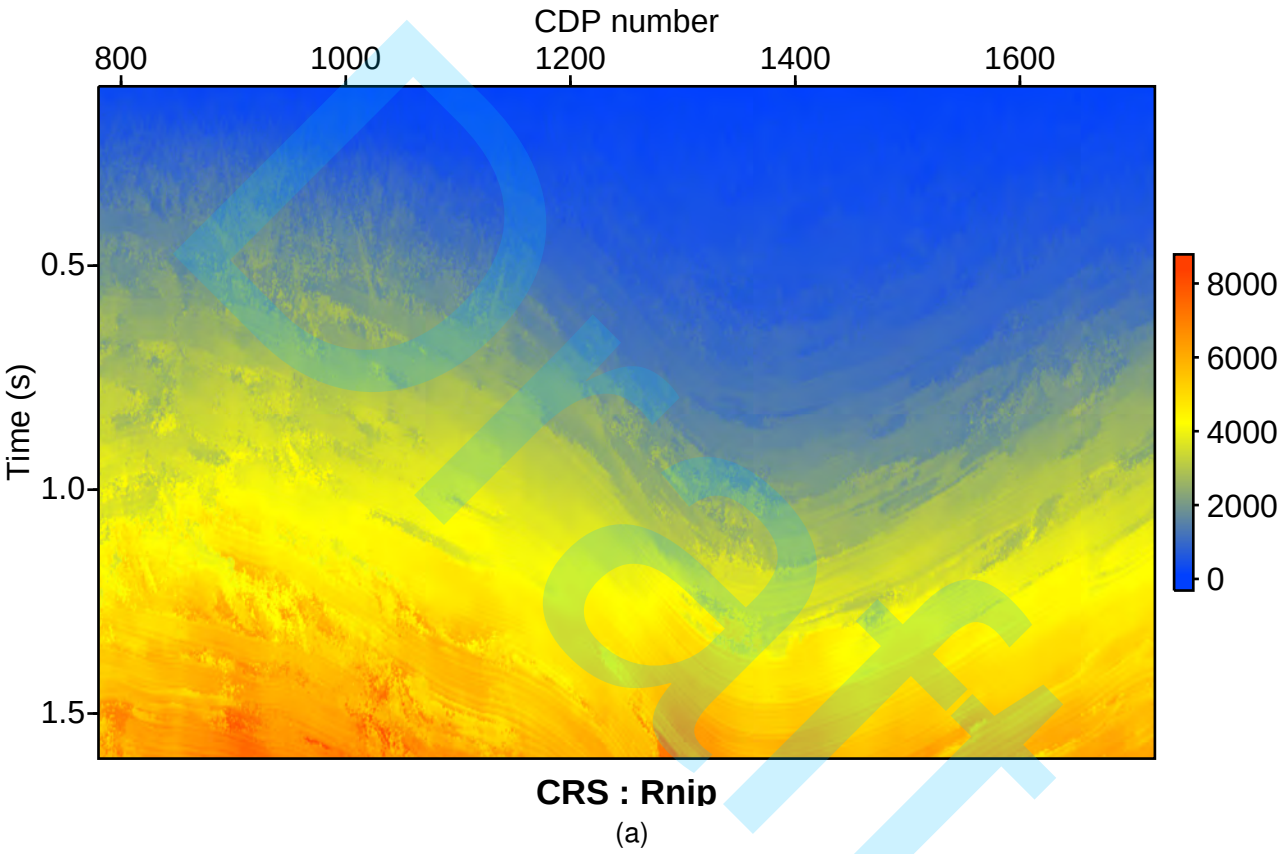

Figure 6. NIP-wave (Rnip) sections from CRS attributes determined from a) original data, b) preconditioned data with MWNI method and c) preconditioned data with MPFI method. The CRS attributes obtained from the MWNI data (b) show less noise interference.

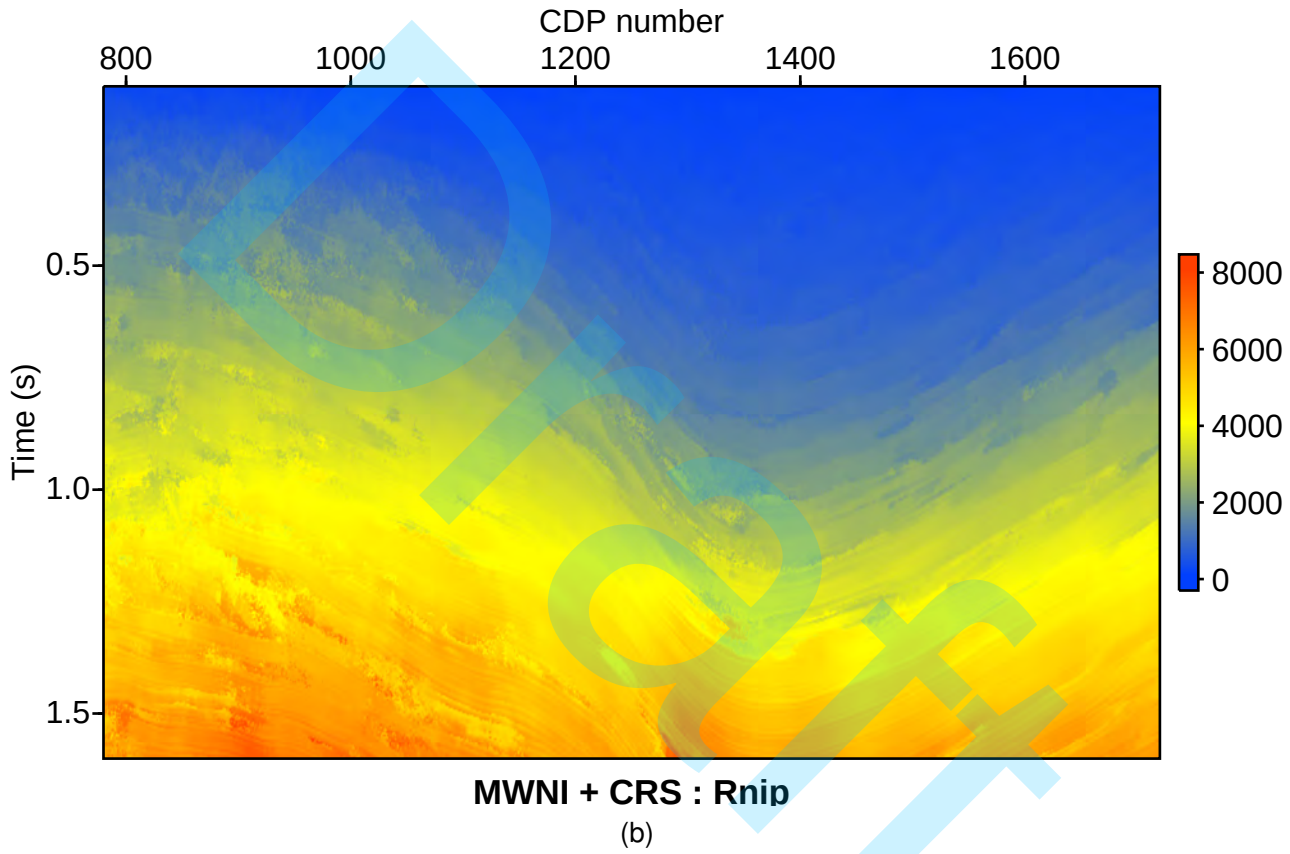

Figure 6. NIP-wave (Rnip) sections from CRS attributes determined from a) original data, b) preconditioned data with MWNI method and c) preconditioned data with MPFI method. The CRS attributes obtained from the MWNI data (b) show less noise interference.

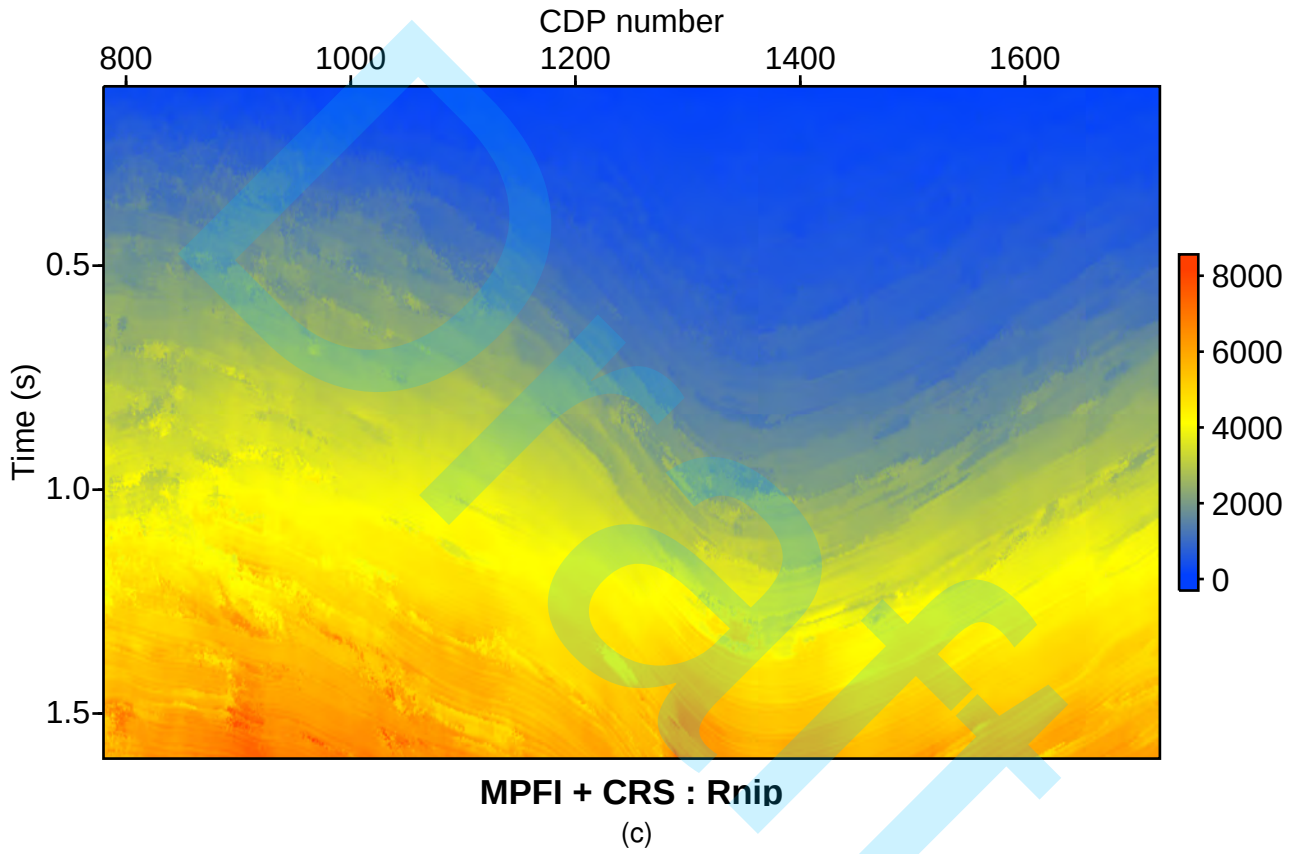

Figure 6. NIP-wave (Rnip) sections from CRS attributes determined from a) original data, b) preconditioned data with MWNI method and c) preconditioned data with MPFI method. The CRS attributes obtained from the MWNI data (b) show less noise interference.

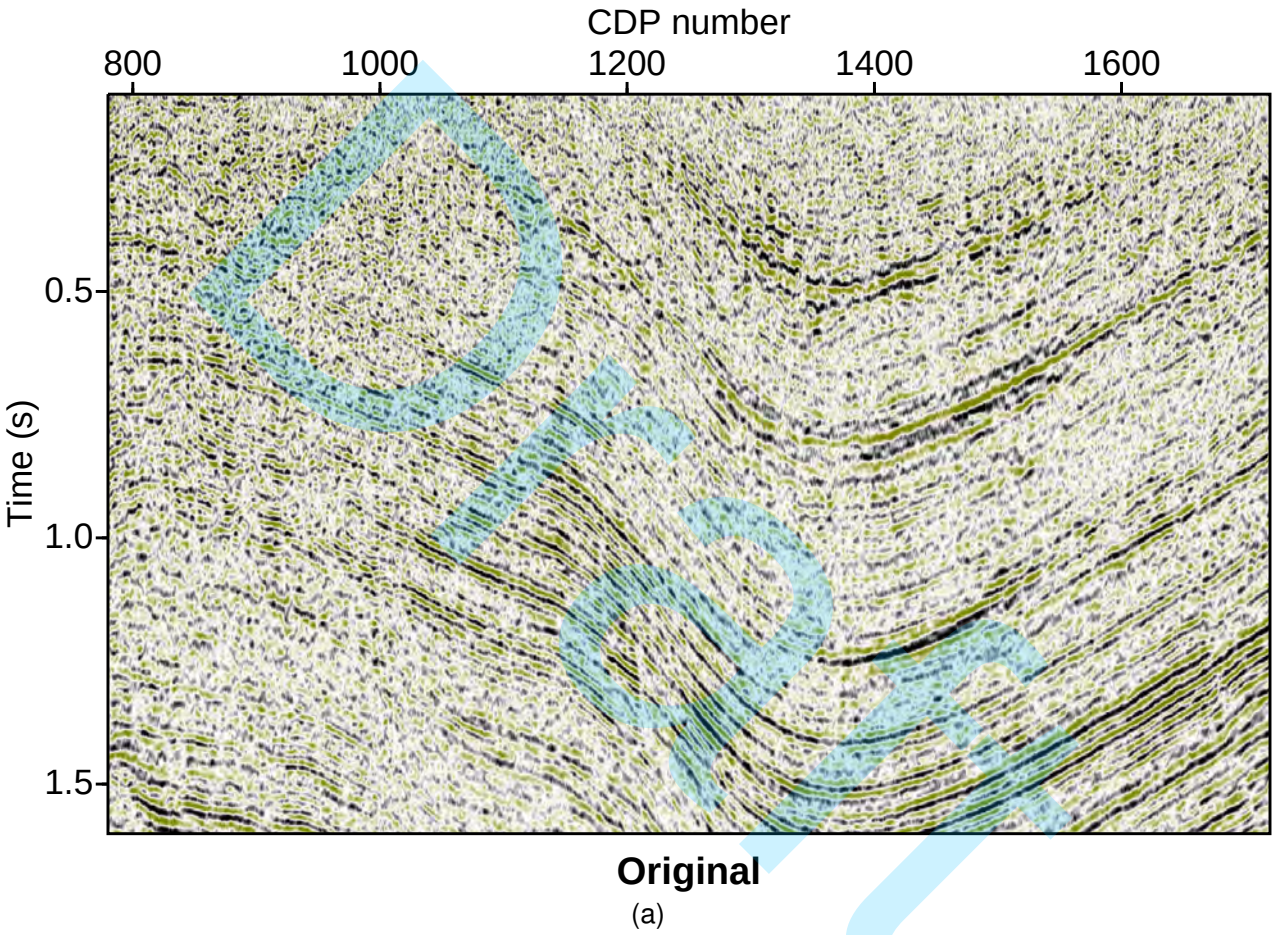

Figure 7. PSTM images of the Tacutu basin obtained from: a) original data, b) MWNI reconstruction, c) MPFI reconstruction, d) CRS reconstruction, e) MWNI + CRS Interpolation, f) MWNI + CRS Denoising, g) MPFI + CRS Interpolation and h) MPFI + CRS Denoising.

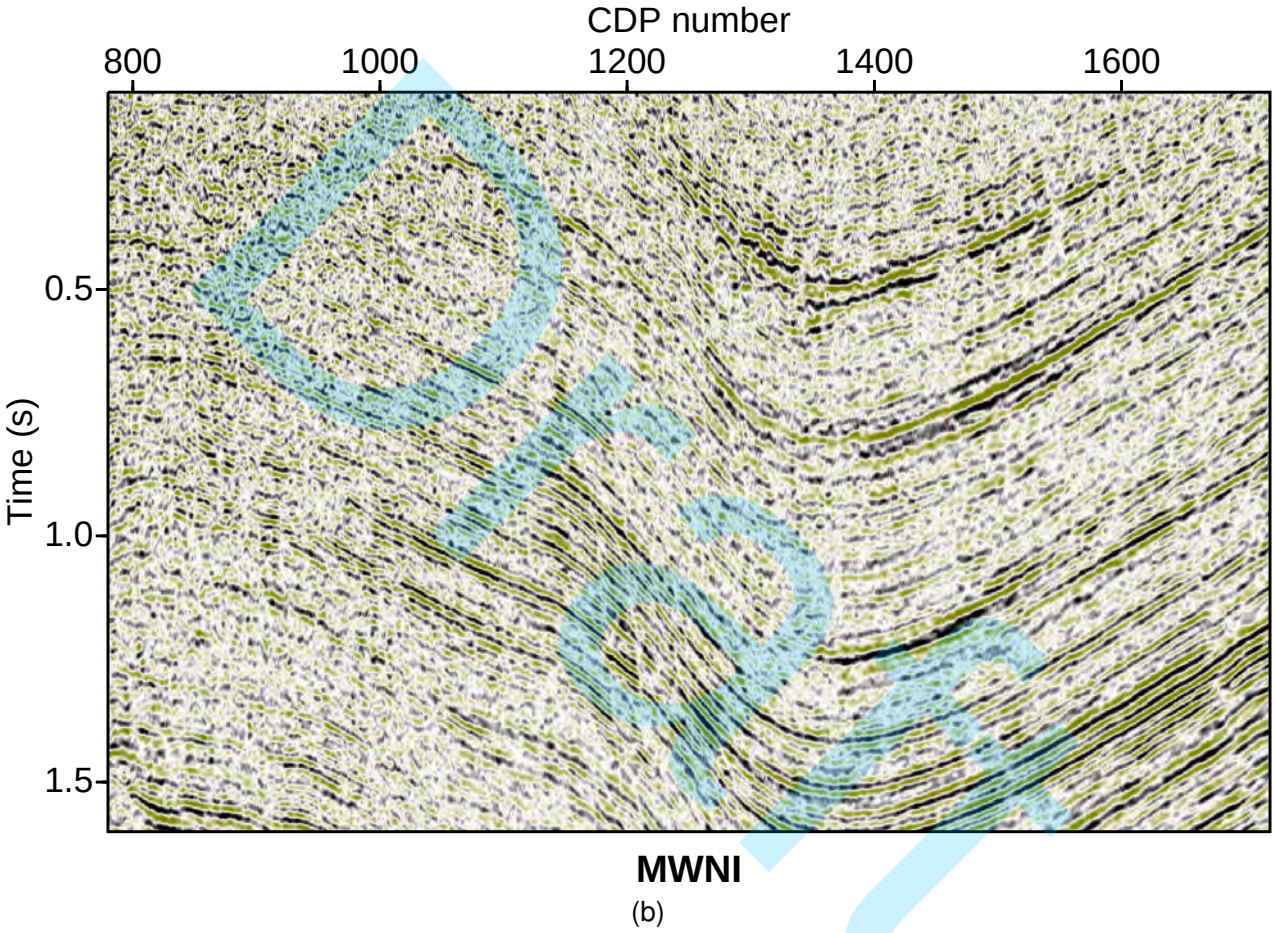

Figure 7. PSTM images of the Tacutu basin obtained from: a) original data, b) MWNI reconstruction, c) MPFI reconstruction, d) CRS reconstruction, e) MWNI + CRS Interpolation, f) MWNI + CRS Denoising, g) MPFI + CRS Interpolation and h) MPFI + CRS Denoising.

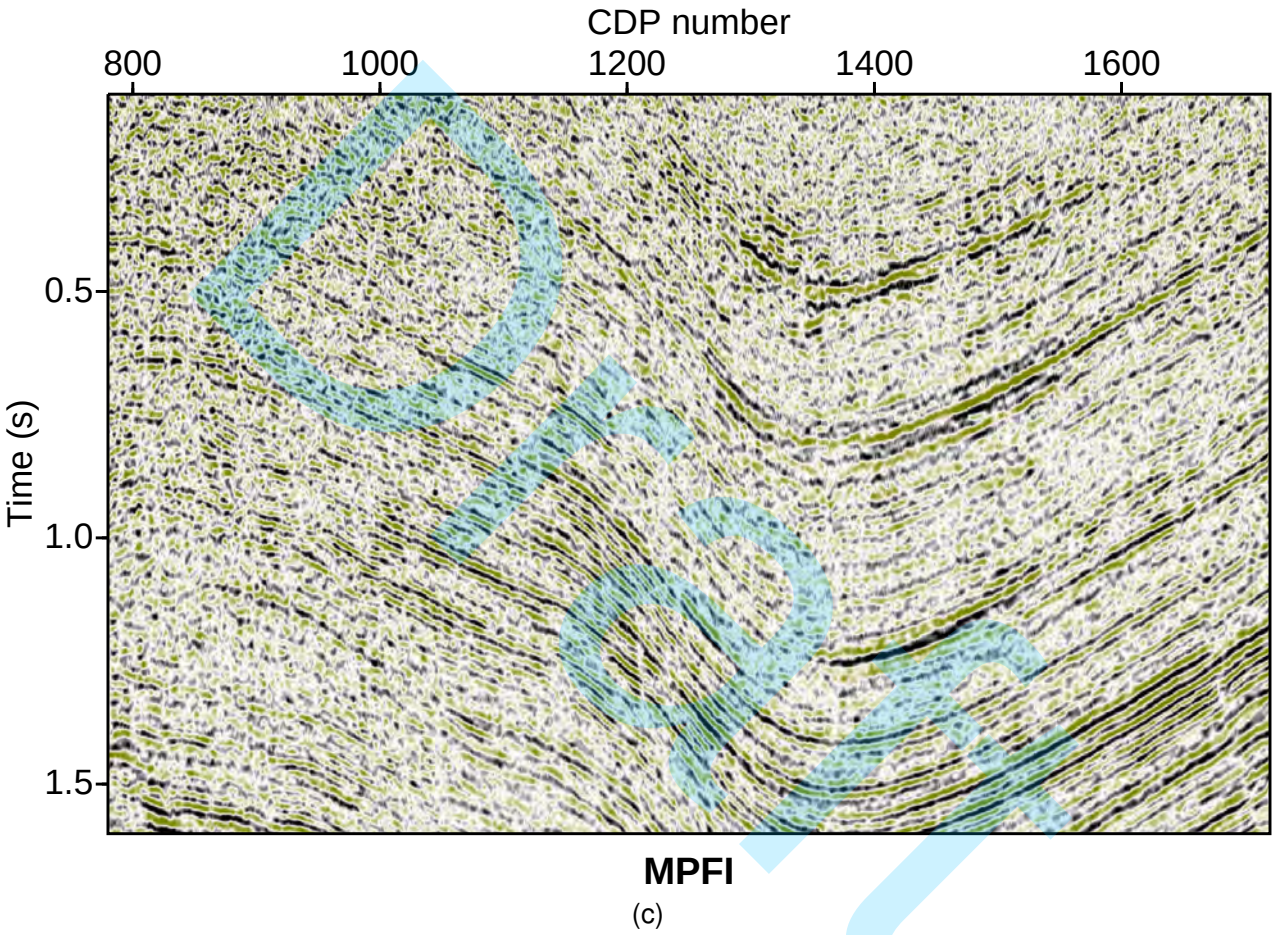

Figure 7. PSTM images of the Tacutu basin obtained from: a) original data, b) MWNI reconstruction, c) MPFI reconstruction, d) CRS reconstruction, e) MWNI + CRS Interpolation, f) MWNI + CRS Denoising, g) MPFI + CRS Interpolation and h) MPFI + CRS Denoising.

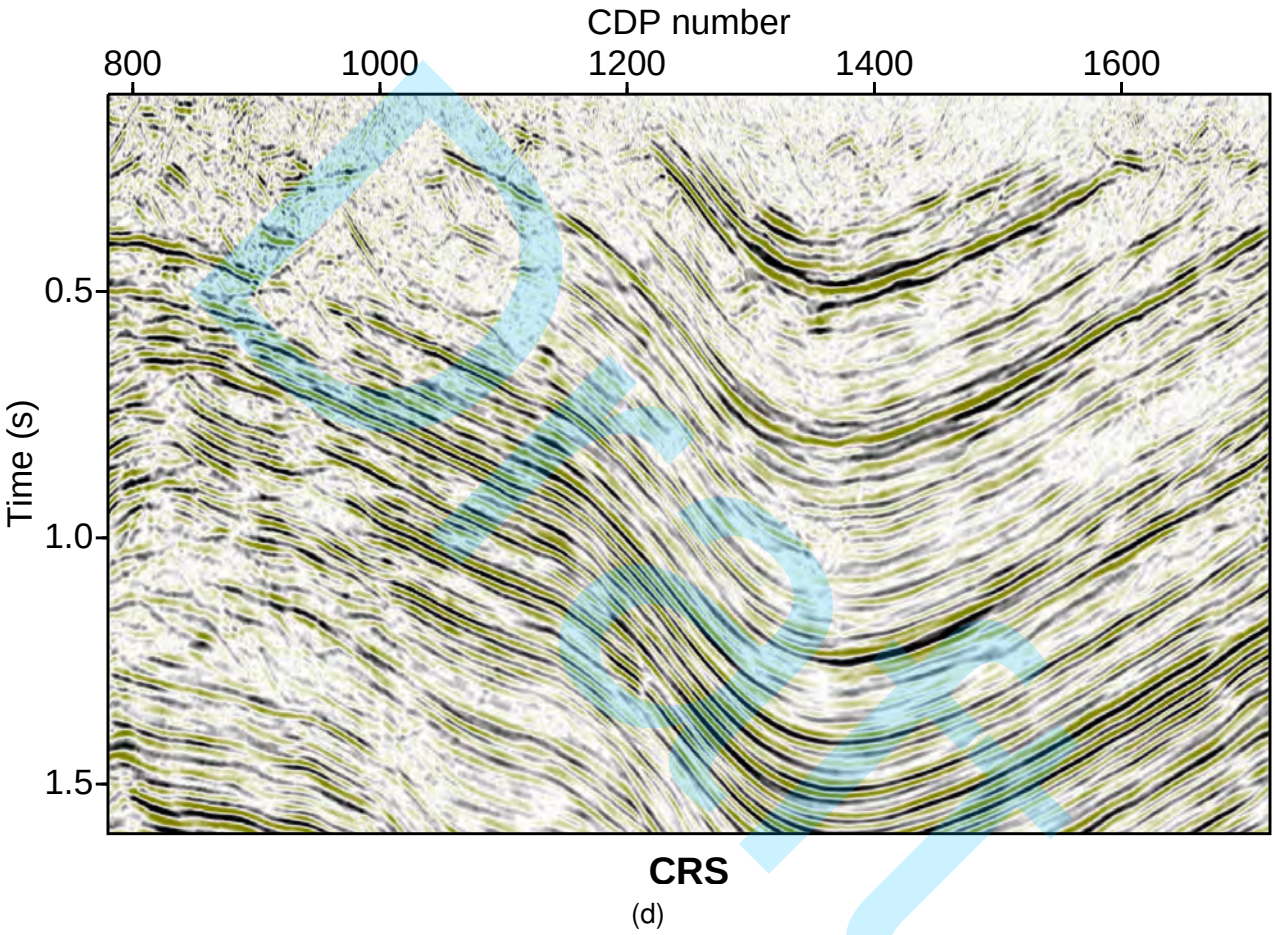

Figure 7. PSTM images of the Tacutu basin obtained from: a) original data, b) MWNI reconstruction, c) MPFI reconstruction, d) CRS reconstruction, e) MWNI + CRS Interpolation, f) MWNI + CRS Denoising, g) MPFI + CRS Interpolation and h) MPFI + CRS Denoising.

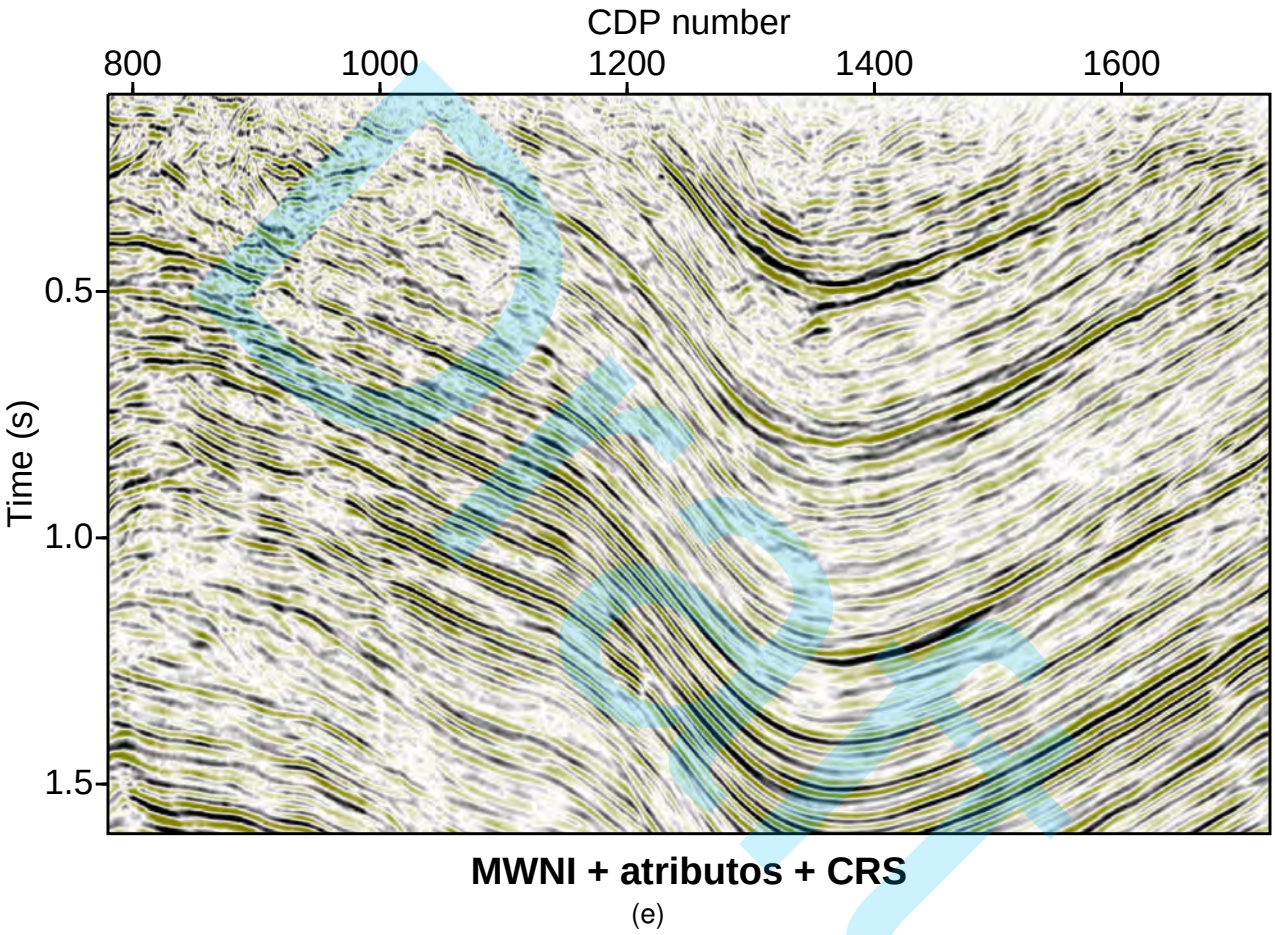

Figure 7. PSTM images of the Tacutu basin obtained from: a) original data, b) MWNI reconstruction, c) MPFI reconstruction, d) CRS reconstruction, e) MWNI + CRS Interpolation, f) MWNI + CRS Denoising, g) MPFI + CRS Interpolation and h) MPFI + CRS Denoising.

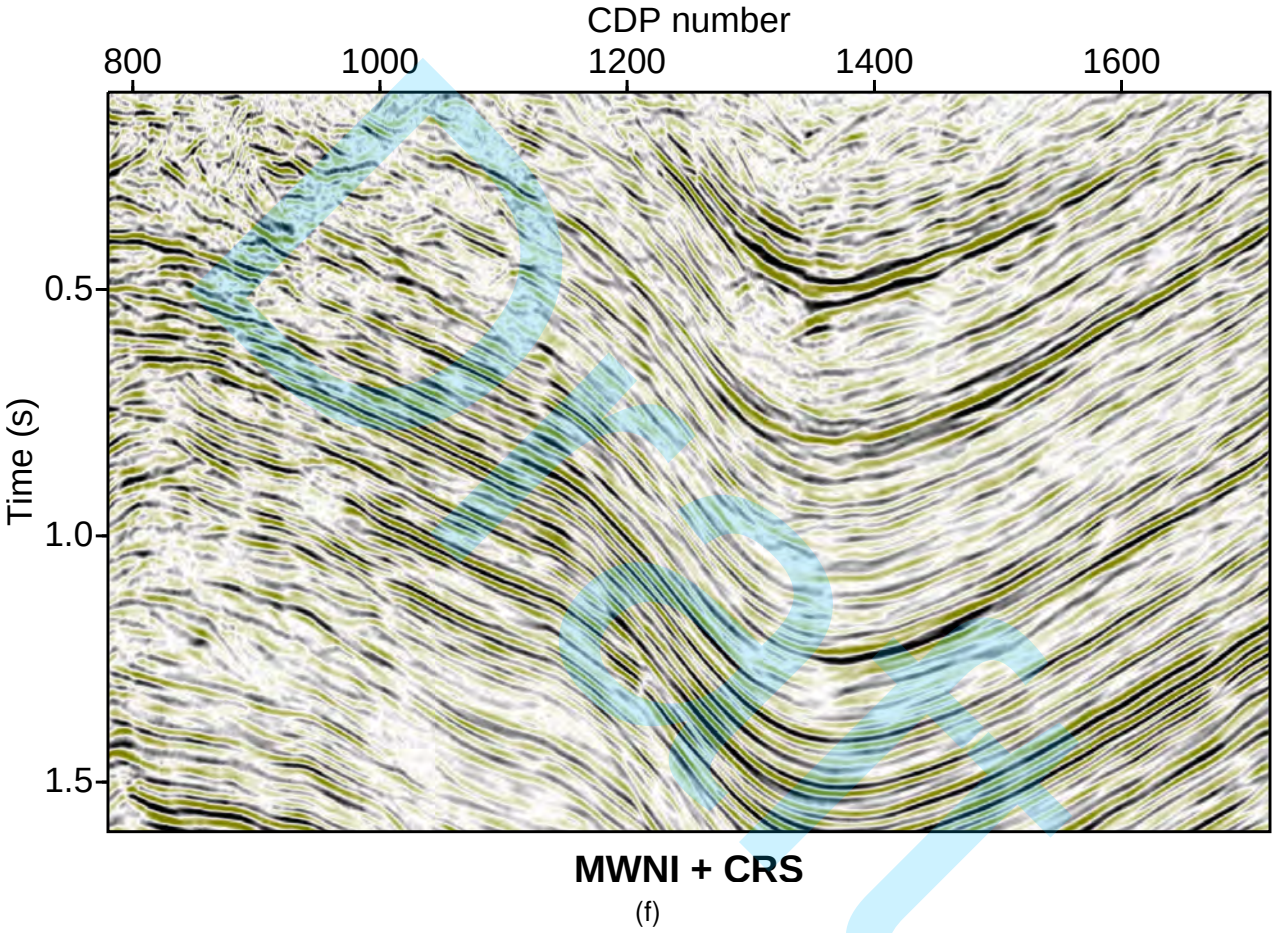

Figure 7. PSTM images of the Tacutu basin obtained from: a) original data, b) MWNI reconstruction, c) MPFI reconstruction, d) CRS reconstruction, e) MWNI + CRS Interpolation, f) MWNI + CRS Denoising, g) MPFI + CRS Interpolation and h) MPFI + CRS Denoising.

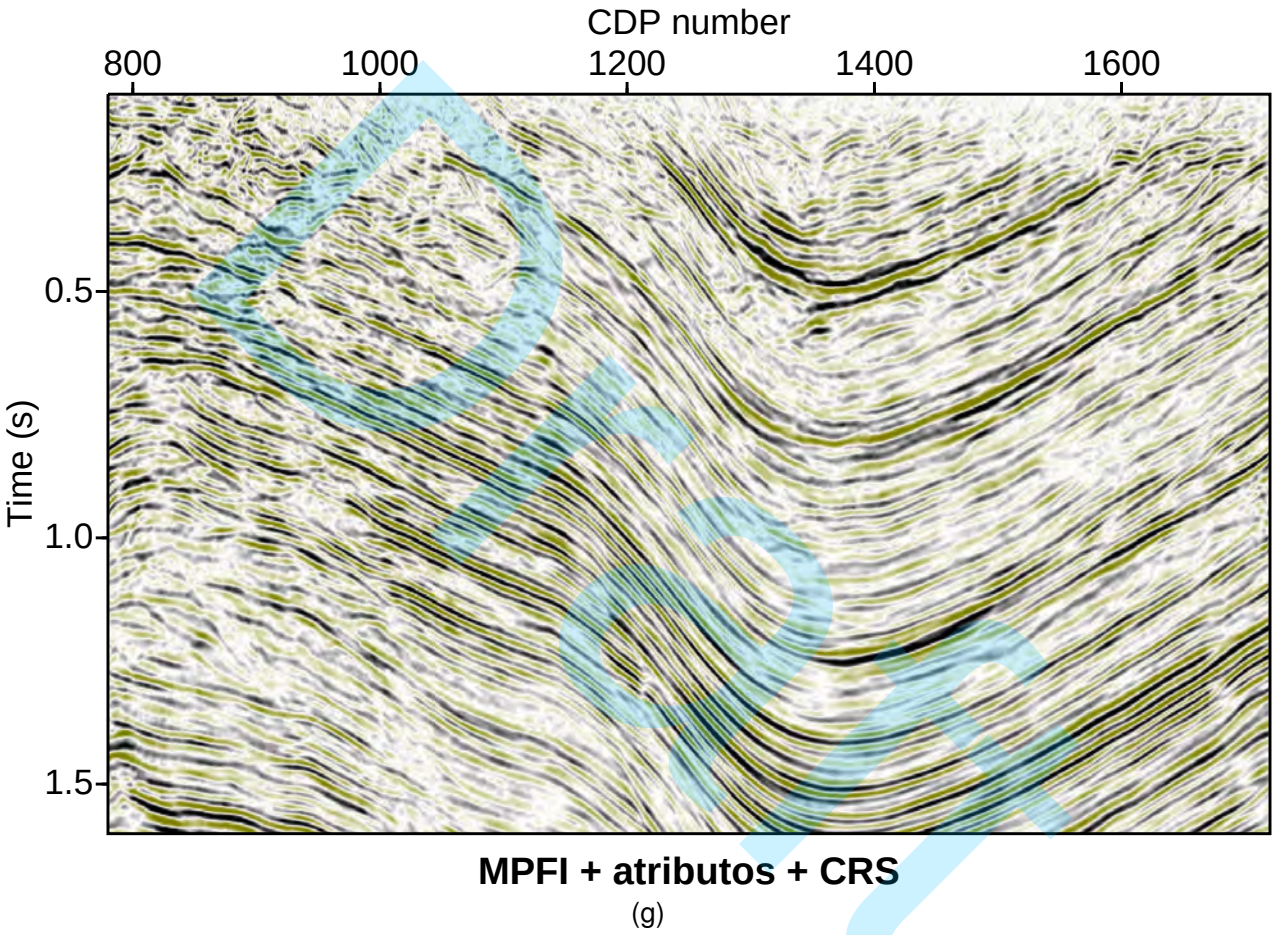

Figure 7. PSTM images of the Tacutu basin obtained from: a) original data, b) MWNI reconstruction, c) MPFI reconstruction, d) CRS reconstruction, e) MWNI + CRS Interpolation, f) MWNI + CRS Denoising, g) MPFI + CRS Interpolation and h) MPFI + CRS Denoising.

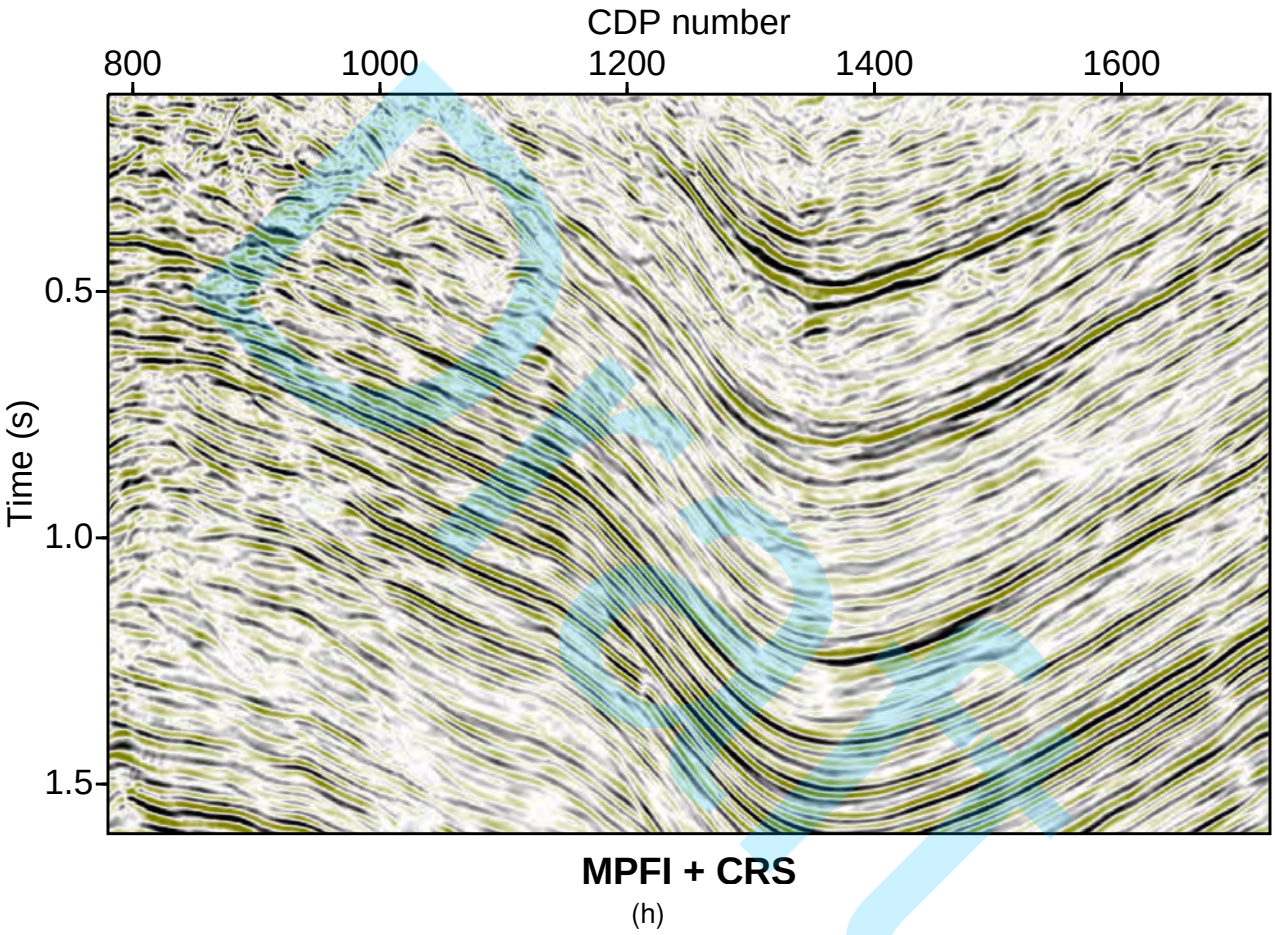

Figure 7. PSTM images of the Tacutu basin obtained from: a) original data, b) MWNI reconstruction, c) MPFI reconstruction, d) CRS reconstruction, e) MWNI + CRS Interpolation, f) MWNI + CRS Denoising, g) MPFI + CRS Interpolation and h) MPFI + CRS Denoising.